A Climate Model Study of the Role of Global Climate in the Late Pleistocene Migration of Anatomically Modern Humans Out of Africa

By

Shannon Leigh Carto

B.Sc., University of Waterloo, 2003

A Thesis Submitted in Partial Fulfillment of the
Requirements for the Degree of

MASTER OF SCIENCE

in the School of Earth and Ocean Sciences

A Climate Model Study of the Role of Global Climate in the Late Pleistocene Migration of Anatomically Modern Humans Out of Africa

By

Shannon Leigh Carto

B.Sc., University of Waterloo, 2003

Supervisory Committee

Dr. Andrew Weaver
Supervisor

Dr. Yin Lam
Co-Supervisor or Departmental Member

Dr. Kartrin Meissner
Departmental Member

Dr. Stephen C. Lonergan
Outside Member

Additional Member

Supervisory Committee

Dr. Andrew Weaver
Supervisor

Dr. Yin Lam
Co-Supervisor or Departmental Member

Dr. Kartrin Meissner
Departmental Member

Dr. Stephen C. Lonergan
Outside Member

Additional Member

ABSTRACT

According to the "Out-of-Africa 2" theory of human evolution all living humans today descend from a group of Anatomically Modern Homo *sapiens* or Anatomically Modern Humans that evolved in Africa 200,000 years ago and subsequently migrated out of Africa and spread into the rest of the World around 100,000 years. As a result an interest has developed in establishing a concrete theory of the factors that compelled and/or motivated our ancestors to venture out of their African origins at this time. Interestingly, the Earth's Last Glacial Cycle also dates from this period--stretching from 115,000 to 10,000 years ago. Current paleoclimate evidence suggests that the climatic repercussions of this glacial cycle in Africa resulted in a shift towards a drier and somewhat cooler climate state and the fragmentation of the formerly extensive forested African landscape. As a result, theories of early human migration have cited African climate change during the late Pleistocene as a determinant; however, the mechanisms responsible for the development of hyper-arid conditions in Africa at this time have remained unresolved.

Although, past global climate change has been ascribed to changes in radiative forcing and changes in atmospheric carbon dioxide, recent paleoclimate studies have revealed that African climate is sensitive to changes in SSTs in the Atlantic, as it appears

that subtropical Africa was more arid when North Atlantic sea surface temperatures (SSTs) were cold during glacial periods. The forcing mechanism believed to be responsible for the development of these cold SSTs are the so-called Heinrich Events that are documented as massive surges of icebergs (from high-latitude ice sheets) into the North Atlantic Ocean during high-latitude glaciations. These Heinrich events resulted in the release of large quantities of freshwater into the North Atlantic, which in turn led to a weakening on the global ocean thermohaline circulation and widespread cooling throughout the region. In particular, marine sediment records from the Nordic Sea document a widespread cooling and ice-rafting event that occurred around 105 kya, known as Heinrich event 9.

In order to investigate the climate processes responsible for promoting cooler and drier conditions in Africa during the migration event of AMH (around 100 kya) I used the University of Victoria Earth System Climate Model (UVic ESCM) to conduct two climate model experiments that compared the global-scale response of climate at 105 kya, in particular the Atlantic Ocean and the African climate system, to: 1) orbitally-controlled solar radiation and atmospheric carbon dioxide forcing appropriate for 105 kya and 2) the combined effect of orbitally-controlled solar radiation and atmospheric carbon dioxide at 105 kya, and North Atlantic freshwater forcing. The ultimate goal of this study is to understand how low-latitude and high-latitude climate processes affect the African climate.

Overall the comparative analysis of these two climate model states revealed that the complex interaction between orbitally-controlled solar radiation and atmospheric CO_2 forcing at 105 kya produced a significant part of the cooling and drying in Africa at this time interval. However, the model also indicated that the climate perturbations, caused by the freshwater forcing, amplified the cooling and drying that was already taking place in Africa due to orbital and CO_2 forcing. Guided by paleoclimate data, archaeological data and the results of this study, I consider it likely that the development of hyper-arid conditions in Africa around 100 kya served as the impetus for the migration event of AMH out of Africa, as these climate changes would have rendered Africa unsuitable for

hominid occupation at this time. These climate model results also provide compelling evidence that high-latitude cold events, induced by Heinrich Events, are strongly covariant with African aridity, and thus provide support to previous assertions that North Atlantic climate changes can be effectively propagated throughout the globe to produce seemingly simultaneous climate change.

Table of Contents

List of Tables

List of Figures

Acknowledgements

I wish to thank my supervisor Dr. Andrew Weaver for the opportunity to attain my Masters degree under his supervision and for enabling me to fulfill my aspirations. I would also like to thank him for the guidance and mentorship he provided throughout my graduate career. I am also very grateful to Ed Wiebe, Michael Eby and the rest of the climate lab for their assistance and guidance; my deepest gratitude to Dr. Renee Hetherington for the time, knowledge and mentorship she provided.

I would also like to thank my family and friends for their unending love, support and encouragement; my deepest appreciation to Annette and Colyn Carto for the sacrifices and efforts they made to ensure my success academically and personally. I would also like to thank Candice Carto-Powell and Abid Aslam for their endless belief in my abilities and their constant words of encouragement.

"There is one thing even more vital to science than intelligent methods; and that is, the sincere desire to find the truth, whatever it, may be"
~ Charles Pierce~

1.0 INTRODUCTION

In our society there is perhaps no other question that has plagued modern science more than the question of where modern humanity originated, and as a result this inquiry into our origins has become one of the most fiercely debated scientific subjects of our time. Although many contrasting views of human evolution have been forwarded, over the years the cumulative weight of both genetic and archaeological evidence has fallen in favour of the theory of human evolution that states that humans evolved from primates deep within the jungles of Africa between 7 - 5 million years ago (7-5 Mya). Scientists refer to these early human species as *australopithecines*[1]. Over the next millions of years our early human-like ancestors, generally referred to as hominins[2], continued to evolve and acquire the abilities to walk upright and think cognitively, all the while remaining confined to the African continent. Over the period of time that hominins evolved, local tectonics, global climate shifts and orbitally-induced insolation changes were influencing the African climate, each working at different timescales, but together producing a unique and highly variable environment. During the mid to late Pliocene epoch (3.6 to 1.8 Mya), during which early hominin evolution took place, arid communities became established in Africa (Adams, 1997). However, it was not until 2 Mya that the increasing degree of aridity in Africa began to significantly affect the development of the lifestyles and habits of these hominins forcing major geographical range expansions and, for the first time, intercontinental migrations. The modern consensus is that the first major migration event out of Africa was carried out by a hominin species known as *Homo erectus* (upright man)[3], which appeared in sub-Saharan Africa around 1.9 Mya and subsequently migrated out of Africa around 1.8 Mya (Gabunia et al., 2000), a theory referred to in the literature as "Out-of-Africa 1". It is alleged that these migrating members of *Homo erectus (H. erectus*) took a southerly route out of Africa eventually crossing into Asia and their eventual destinations: China and what is now Indonesia (Gabunia et al., 2000). Based on this theory, it is thought that *H. erectus* gave rise to the hominin species *Homo sapiens neanderthalensis* in Europe around 300,000 years ago (300 kya), whereas in Asia, species of *H. erectus* stopped evolving completely.

---

[1] Species of *australopithecines* lived between 4 and 2 million years ago. They exhibit a variety of adaptations that mark the transition from ape to human.

[2] A taxonomic group including *Homo sapiens* and their ancestral relative species, extending back in time until the split with the line leading to chimpanzees.

[3] Some authors believe that *H. ergaster* evolved into *H. erectus* while migrating into Eurasia. Some recognize them as two sister species: erectus is assigned to the Eurasian specimens, while *H. ergaster* is reserved for those from Africa.

In the literature *H. erectus* is regarded as the first pandemic hominin species; however, most anthropologists agree that this migration was followed by another major migration event around 100 kya by a new species of hominin, our direct ancestors, Anatomically Modern *Homo sapiens* or Anatomically Modern Humans (AMH). It is believed that AMH eventually emerged in Africa around 200 kya from the evolving stream of hominins that had remained in Africa after the African exodus of *H. erectus* (Stringer & Andrews, 1988). This theory also posits that around 100 kya AMH spread out of Africa and into other regions of the World, a dispersal that purportedly replaced all existing populations of non-modern humans (*Homo erectus and Homo sapiens neanderthalensis*) living across Africa and Eurasia (Stringer & Andrews, 1988). This theory is referred to in the literature as "Out-of-Africa 2". The central tenet of the "Out-of-Africa 2" theory is that these early AMH eventually gave rise to all humans living throughout the globe today.

Over the years, opposition to the "Out-of-Africa 2" theory has emanated from the fact that there is great disagreement over the geographical origins of the first AMH. It is presently contended by some that present-day human populations worldwide evolved independently in Europe, Asia and Africa from regionally dispersed populations of *H. erectus*, with *H. sapiens neanderthalensis* being a phase in the development of AMH outside of Africa. This theory is referred to in the literature as the "Multi-Regional Theory" of human evolution (Thorne and Wolpoff, 1992). Implicit in the "Multi-Regional Theory" is the failure of any subsequent population expansion out of Africa, and thus the implication that present-day human populations are all descended from a single migration event out of Africa executed by members of *H. erectus* 1.8 Mya. This issue has been addressed through the study of fossil and archaeological records, as well as genetic studies that attempt to reconstruct the evolutionary history of humans based on the examination of patterns of genetic diversity within and between populations of living humans (Foley, 1998; Quintana-Murci et al., 1999). Over the years this growing body of evidence has fallen in favour of the "Out-of-Africa 2" theory of human evolution, and discussion is now focused on establishing a concrete theory of the circumstances and/or factors that allowed or compelled AMH to suddenly migrate out of their African origins at this time.

Recently, a number of theories have proposed that climate-driven environmental changes in Africa may have played an integral role in early human range dynamics and migrations (Vrba, 1995; Behrensmeyer and Chapman, 2002; Tiedemann et al., 1994). In general, long-term

precipitation changes throughout the African continent, influenced by the African monsoon (from the West) and the Indian monsoon (from the East), are thought to be governed by precessional variations in summer insolation (23 –19 kyr period) (Kutzbach & Liu, 1997; Partridge et al., 1997). However, the recent analysis of paleoclimate evidence from Africa and its adjacent oceans has revealed that the African continent experienced periods of extreme hyper-aridity superimposed on the long-term waxing and waning of the monsoon which cannot be explained exclusively by changes in insolation (Hoelzmann et al., 2004, deMenocal, 1995; deMenocal, 2004). These paleoclimate records have helped shed new light on the migratory history of early hominins by revealing that both before and during these migrations the African climate began to shift towards progressively arid conditions. These changes took place in tropical and subtropical Africa, the essential geographical area from which hominins, including AMH, originated and dispersed from.

The recorded periods of African hyper-aridity appear to occur in tandem with the initial growth and subsequent expansion of high-latitude ice sheets during the Pliocene-Pleistocene glacial periods (deMenocal, 2004). Moreover, it appears that after the 200 kya-mark African glacial stages were more arid than those of the middle Pleistocene (781 –126 kya) (Jahns et al., 1998). In the case of the migration event of AMH, the Last Glacial Cycle also dates from this period--stretching from 115 to 10 kya (late Pleistocene epoch). Current paleoclimate evidence suggests that the climatic repercussions of this glacial cycle in Africa resulted in a shift towards a drier and somewhat cooler climate state and the fragmentation of the formerly extensive forested African landscape (Adams & Faure, 1997). Furthermore, the fall and subsequent rise of sea level occurred repeatedly during this time, coinciding with the expansion and melting of glaciers. As sea level fell, coastal land expanded, which led to the development of land bridges between continents and islands. In addition, the analysis of trapped air bubbles in ice cores have also shown that at the peak of glacial phases, atmospheric CO_2 concentration was about 30% lower than during interglacial conditions (Jouzel et al., 1993). Computer climate simulations suggest that the lower carbon dioxide concentrations would directly cool the atmosphere, and cause the world to cool by less than 1° C on average (Houghton et al.,1995). Moreover, climate models have also shown that changes in atmospheric carbon dioxide feedback to amplify orbitally induced changes in solar radiation (Hughes and Weaver, 1994).

Interestingly, paleoclimate studies have also revealed that the development of hyper-arid conditions in Africa were particularly synchronous with cold North Atlantic Sea Surface Temperatures (SSTs) that occurred during high-latitude glacial periods (deMenocal, 1995). In accord with these paleoclimate records, modern occurrences of African Sahelian drought have also been related to cold SSTs in the North Atlantic (deMenocal, 1995). A key question surrounding this climate scenario that links African climate to high-latitude cold events concerns the mechanisms that are responsible for the inter-hemispheric connections. One of the most discussed hypotheses relies on the fact that current surface water paleoclimate records from the North Atlantic have shown that over the last 150,000 years (150 kyr), cold SSTs in the North Atlantic have been associated with short-lived but massive discharges of icebergs from the circum-Atlantic ice sheets into the North Atlantic Ocean during glaciations, known as Heinrich events (HE) (Dowdeswell et al., 1995; Heinrich, 1988). Several studies have documented that the development of cold North Atlantic SSTs during these HE is attributed to the impact that these events have on the strength of the global ocean thermohaline circulation (THC). The ocean THC is primarily controlled by the magnitude of the North Atlantic Deep Water (NADW) production. At present, warm and salty tropical water is carried to the high-latitudes in the North Atlantic Ocean (carrying with it tremendous amounts of heat). As it moves northward, this water loses its heat to the atmosphere causing the surface waters to cool and become more saline (due to brine rejection during the formation of ice sheets), this water therefore becomes sufficiently dense enough to sink and become NADW, thus beginning the global deep-ocean conveyor system. This process is thought to play a crucial role in driving the global ocean circulation and in regulating global climate.

It has been suggested that the THC was reduced during glacial periods due to the input of freshwater from melting icebergs during HE, which created a low-salinity cap over the North Atlantic that inhibited sinking of NADW and caused widespread cooling within the North Atlantic region (Rahmstorf, 2003; Fanning and Weaver, 1997). In particular, marine sediment records from the Nordic Sea document that a widespread cooling and ice-rafting event occurred around the time of the putative migration event of AMH, labelled as HE 9 that occurred around 105 kya (McManus et al. 1994). Although these paleoclimate results lend new support to hypotheses of a climate link between high-and low-latitudes during glacial periods, and hypotheses of a climate-driven migration of AMH, the difficulty has been identifying the climate mechanisms responsible for this

climate evolution in Africa and proving that these African climate changes triggered a response in AMH.

Although no concrete theory exists for understanding the mechanisms of past climate change in Africa, these paleoenvironmental and climate model studies set the large scale spatial and temporal scenario for assessing the cause of the aridification of Africa during the late Pleistocene, and reconciling the conspicuous temporal relationship between the shifts in African climate and the African exodus of AMH. In order to improve these theoretical frameworks this study begins by presenting a coherent picture of the available paleoclimate and archaeological evidence that supports the assertion that the migration events of *Homo erectus* and AMH can be linked to African climate change, namely the development of a cooler and drier climate. Secondly, focusing solely on the climatic circumstances surrounding the migration event of AMH, this study investigates the climate processes responsible for promoting cooler and drier conditions in Africa around 100 kya by using the University of Victoria Earth System Climate Model (UVic ESCM). This study presents the results of two climate model experiments that compared the global-scale response of climate at 105 kya, in particular the Atlantic Ocean and the African climate system, to: 1) orbitally-controlled solar radiation and atmospheric carbon dioxide forcing appropriate for 105 kya and 2) the combined effect of orbitally-controlled solar radiation and atmospheric carbon dioxide at 105 kya, and North Atlantic freshwater forcing. The ultimate goal of this study is to investigate whether (one, if not both, of) these forcing regimes are able to produce sufficient cooling and drying of the African continent that compares favourably to the paleoclimate data. Guided by archaeological datasets, paleoclimate datasets and the climate model results of this study, it is argued here that the evidence strongly suggests that shifting environmental conditions in Africa contributed to the migration event of AMH, and that the development of these climate shifts, namely shifts towards a progressively cooler and drier climate around 100 kya, can be ascribed to both high-and low-latitude climate processes that were in operation during the late Pleistocene.

The central tenet of this study is that the history of early human demography and migration can ultimately be explained in terms of fundamental climate changes in Africa. This concept, provides not only a consistent framework to understand the fundamental processes and patterns by which human expansion outside Africa began and evolved towards other continents, but also to understand the mechanisms for propagating climate signals between high-and low-latitudes. The

motivation for performing freshwater forcing experiments, such as this one, stems from the century-old theory that millennial-scale climate changes are driven by rapid influxes of freshwater into the North Atlantic from the melting of continental ice sheets during HE (Broecker et al., 1985). Although elements of high-latitude climate change are relatively well understood during HE, the response of low-latitude climate to freshwater forcing has remained for the most part unknown.

At present, the literature is full of theories that propose that there may have been multiple migrations out of Africa, in addition to the two mentioned here (Foley and Lahr, 1994). However, the number of proposed successful hominin dispersals from Africa into Eurasia varies depending on the author's interpretation of the archaeological evidence. As a result of the inherent ambiguity in the interpretation of the fossil record, the scope of this study is confined to establishing the role of climate in the migration events of *Homo eretcus* and AMH, and further investigating the climate processes responsible for the aridification of the African continent during the migration event of AMH by using the UVic ESCM. This study focuses predominantly on the migration event of AMH as it is believed that this migration event holds the keys to understanding the origins of humanity and how human diversity developed worldwide.

2.0 BACKGROUND: The African Exodus of *Homo erectus* in the context of Pliocene-Pleistocene Global Climate Change

Current evidence suggests that before 3 Mya, the African continent was generally moister than present, with greater forest and tree cover and less desert (PRISM project members, 1996). However, around 3 Mya, the African environments began to shift more towards a drier and somewhat cooler climate state (Adams & Faure,1997). In this time interval, pollen and other evidence suggests more widespread grasslands in east Africa, scrub vegetation in southern Africa, and extension of desert in North Africa (Adams, 1997). According to pollen, dust and isotope indicators of arid conditions, these conditions continued to generally increase into the Quaternary period, during most of which environments were cooler and more arid than at present (Finlayson, 2004). According to paleoclimate evidence recorded in marine sediment sequences recovered from dust plumes off the western and eastern margins of subtropical North Africa, during the mid to late Pliocene epoch (3.0 -1.8 Mya) subtropical Africa experienced progressive, step-like increases in aridity (deMenocal, 1995). The marine sediment records analyzed in deMenocal (1995)'s study contain several well-dated continuous records of wind-borne (eolian) dust variability from the African continent, which are closely related to precipitation anomalies in these African dust source areas (Prospero & Nees, 1986). According to these records of interannual variation in eolian dust concentration from the western and eastern margins of North Africa, northwest Africa, northeast Africa and Arabia suffered cycles of colder, drier climate around 2.8 Mya, 1.7 Mya and 1.0 Mya (deMenocal, 1995; Vrba et al., 1989; Tiedemann et al., 1994). Interestingly, the African climate changes documented by deMenocal (1995) coincide with the onset and subsequent amplification of large North American and European ice sheets and cooling of the subpolar oceans that occurred after 3.0 -2.6 Mya, 1.8 -1.6 Mya and 1.2- 0.8 Mya (deMenocal, 1995; Tiedemann et al., 1994). See Figure 1, for the location of the marine sediment sequences analyzed in deMenocal (1995)'s study, mentioned above.

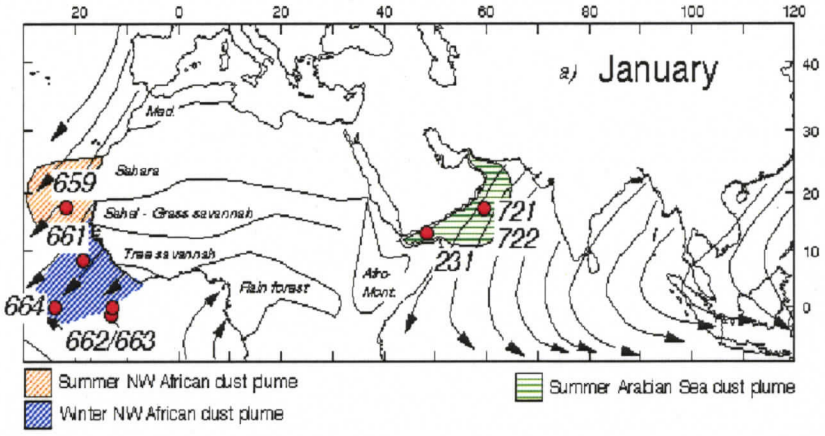

Figure 1: Ocean Drilling Program sites off western and eastern subtropical Africa used to reconstruct African climate during the Pliocene-Pleistocene. (deMenocal, P. B., 1995. Plio-Pleistocene African Climate, Science, 270: 53-59)

In his research, deMenocal (1995) also observed that prior to 2.8 Mya, subtropical African climate varied at the 23-19-kyr period (orbital precession cycle), which has been interpreted to reflect African monsoon climate (deMenocal, 1995). However, after 2.8 Mya, when ice sheets were growing in the Northern Hemisphere, African aridity, as well as high-latitude glacial-interglacial cycles, oscillated on the longer 41-kyr (orbital obliquity cycle). After 1.0 Mya, African eolian cycles shifted to the larger 100-kyr periods (orbital eccentricity cycle), as did the high-latitude glacial-interglacial cycles (Shackleton et al., 1990, Ruddiman et al., 1989, Raymo, 1994). The marine sediment records studied by deMenocal (1995) also revealed that dust layers deposited during times corresponding to high-latitude glaciations tended to be thicker and have higher eolian concentrations than their warm interglacial counterparts. Moreover, it appears from these marine sediment records that glacial interval dust layers were met, especially in the last 1 million years, by abrupt African vegetation distribution changes caused by increased aridity (deMenocal, 1995; Hughen et al., 1996).

These Pliocene-Pleistocene shifts in African climate variability (records of eolian dust deposition off the western and eastern subtropical Africa; deMenocal, 1995 & 2004) and shifts in high-latitude glacial climate ($\delta^{18}O$ ice core records; Tiedemann et al., 1994) are depicted in Figure 2 below (deMenocal, 2004). In Figure 2, the areas outlined in red document progressive shifts in

African climate variability and increasing aridity (increases in dust flux documented in the West African sites 659, 661, 662, 663 and 664 and the East African sites 721/722 indicated in Figure 1) that occur after 3.0 -2.6 Mya, 1.8 -1.6 Mya and 1.2- 0.8 Mya. This figure also documents how these eolian dust records appear to be coeval with the onset and subsequent amplification of high-latitude glacial cycles (deMenocal, 1995; Tiedemann et al., 1994; Clemens et al., 1999).

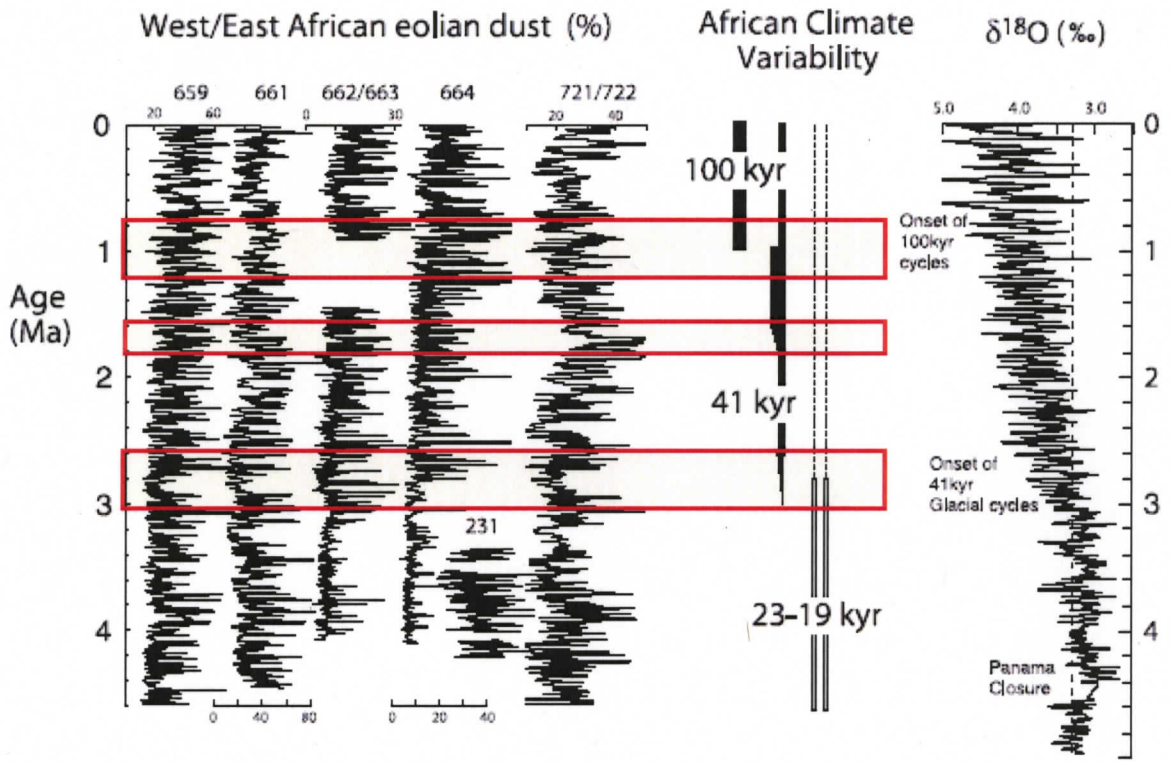

Figure 2: Temporal relationships between Pliocene-Pleistocene changes in African aridity (records of eolian dust deposition at seven Ocean Drilling Program sites off western and Eastern subtropical Africa; see Figure 1) and high-latitude glacial ice volume (Tiedemann et al., 1994; Clemens et al., 1999). (deMenocal, P.B., 2004. African climate change and faunal evolution during the Pliocene-Pleistocene. Earth and Planetary Science, Frontiers, 6976: 1-22)

As mentioned in the introduction, dispersals of early humans from Africa have been a regular feature since the emergence of the species, *H. erectus*, which rapidly dispersed from its origin in sub-Saharan Africa around 1.8 Mya, shortly after its evolution around 1.9 Mya (Gabunia et al., 2000). Despite the difficulties in correlating the paleoclimate and archaeological records,

when examining the spatial and temporal characteristics of this migration event within the context of African paleoclimate at this time, it is evident that the migration of *H. erectus* is contemporaneous with the progressive shift towards more arid and open environments in Africa that took place 3.0 -2.6 Mya, 1.8 -1.6 Mya and 1.2- 0.8 Mya outlined above (deMenocal, 2004). In theory, the initiation of a cooler and drier climate in Africa around 3 Mya would have cleared out some of the woodland to form new open and fragmented habitats, and thus may have acted as a selective force on the more forest-adapted ancestors of *H. erectus* living in Africa (early *Homo*[4]), to develop new physical and behavioural adaptations, which resulted in the evolution of the *H. Erectus* around 1.9 Mya. However, the increasing frequency and degree of cooling and drying that intensified into the Pleistocene may have ultimately led these newly evolved species of *H. Erectus* to adapt by migrating out of Africa, rather than adapting in situ, as their predecessors may have. Thus, the deteriorating environmental conditions that prompted the evolution of *H. erectus* may have also encouraged this species to migrate out of Africa. Furthermore, many African carnivores spread to Eurasia during the early Pleistocene (Vrba, 1995) and these early humans could have moved along with them.

According to the fossil record it appears that adaptations for endurance running also emerged about 2 Mya, in the early species of our own genus, *Homo* (Bramble & Lieberman, 2004). These adaptations include a special arrangements of tendons in our legs (including long Achilles tendons) that can act like springs and large gluteus maximus muscles that are believed to stabilize the trunk of the human body, both of which are not found in apes (Bramble & Lieberman, 2004). According to Bramble and Lieberman (2004), endurance running is the only known behaviour that would account for the difference in body plans in *Homo* as opposed to apes or *australopithecines*. In theory, the increase of open landscape in Africa during the late Pliocene may have not only motivated the evolution of this more modern body form and the ability to do endurance running, but it may have also removed an anatomical and environmental constraint on human range dynamics and migrations.

The examination of the migration of *H. erectus*, as a response to climatic and environmental fluctuations, is of great importance to this study. The time during which this

[4] *Homo* is the genus that includes Anatomically modern humans and their close relatives. The genus is estimated to be between 1.5 and 2.5 million years old. All species except Homo sapiens are extinct.

species evolved and subsequently rapidly migrated out of Africa was marked by climatic changes, namely aridity in the African continent, similar to the climate changes that took place during the last glacial cycle, which I will describe in the next section. By implication, the determination of the climate-link in this migration helps to establish a generalized theory that climate-driven ecological change has long been the driving force in the geographical range dynamics of early humans, and thus that the ensuing migration of AMH is part of a recurring theme in human history.

3.0 Fossil Record of the Emergence and Migration of Anatomically Modern Humans

The current evidence for the dispersal of early AMH from Africa to Asia is derived from discoveries of fossils around the world that have helped scientists to determine the spatial and temporal characteristics of not only the geographical origin of our the first AMH, but also their migration path throughout the world. The oldest remains of AMH have been found at the Omo Kibish formation in Ethiopia dating back to 195 kya (McDougall et al., 2005) and from Herto in Ethiopia dating back to 160 –154 kya (White et al., 2003), suggesting that at the time of their origin AMH populations were restricted to tropical Eastern Africa. AMH remains begin to appear throughout Africa around 125 kya, suggesting that AMH began to expand their geographical range at this time, spreading into North, West and South Africa (Finlayson, 2005). The fossil remains of AMH outside of Africa, though scarce, are now well documented. AMH fossil remains have been found in Skhul and Qafzeh in the Middle East dating back between 115- 92 kya (Bar-Yosef, 1995). Initially the human fossil remains found at these two sites in the Middle East led scientists to believe that AMH had taken a northern route out of Africa along the Nile valley and into Israel. However, the remains not only exhibit many archaic features not indicative of AMH, but they were also found in association with typical African faunal remains (Stringer and Andrews, 1988). As a result the region is considered to be a biogeographic extension of the African continent and it is no longer believed that these fossils represent traces of AMH migrating out of Africa (Stringer and Andrews, 1988). In Australia, the oldest dated AMH fossil remains are the 'Lake Mungo I' remains, which, together with the dating of archaeological sites associated with these remains, suggest that they reached Australia between 45 – 60 kya (Cann et al., 1987). In Eastern Asia, a cave in south China, at Liujiang, has yielded AMH remains dated back to 67 kya (Trinkhaus, 1986). In Europe, the oldest fossil remains of AMH date back to 40 kya, when it appears Neanderthals gave way to AMH (Trinkhaus, 1986). The oldest AMH fossils date back to 12.5 kya in the Americas (North and South America), indicating that they were the last to be colonized (Cann et al., 1987).

3.1 Possible Migration Routes

Given that AMH fossils appear to be much older in Africa than on any other continent, it is presently argued that this implies that at least one dispersal of AMH from Africa occurred during the late Pleistocene. The traditional view has been that AMH colonized the world through an inland route, moving out of Africa northwards through the Levantine corridor and into the Middle East subsequently spreading into Asia, India and the Far East (Stringer, 2000). Once there, they adapted to coastal life and developed boats to get to Australia (Stringer, 2000). In contrast, one view that has gathered recent support is the theory that AMH may have taken a southern coastal route out of Africa, beginning on a route along the Red Sea Coast of East Africa into the Arabian Peninsula perhaps across a land bridge exposed by a drop in sea level (Stringer, 2000; Walter et al., 2000). Continuing along the narrow southern shorelines, it is postulated that they progressed all the way to Indonesia (Stringer, 2000). Although these human migration theories imply the use of coastlines and continental shelves as possible migratory routes out of Africa, the archaeological record, particularly that relevant to coastal adaptations, is likely seriously underrepresented because of the rapidly changing sea-level history of shelf environments and the fact that if there are other coastal sites they remain submerged and unaccessible at present (Erlandson, 2001). As a result, data and/or research are insufficient to provide a meaningful history. In Figure 3, the traditional inland northern migration route (dashed line through Sinai) and the more recently suggested southern coastal migration route (dashed line across the Bab-el-Mandeb Strait) out of Africa are illustrated (Forester and Matsumura, 2005).

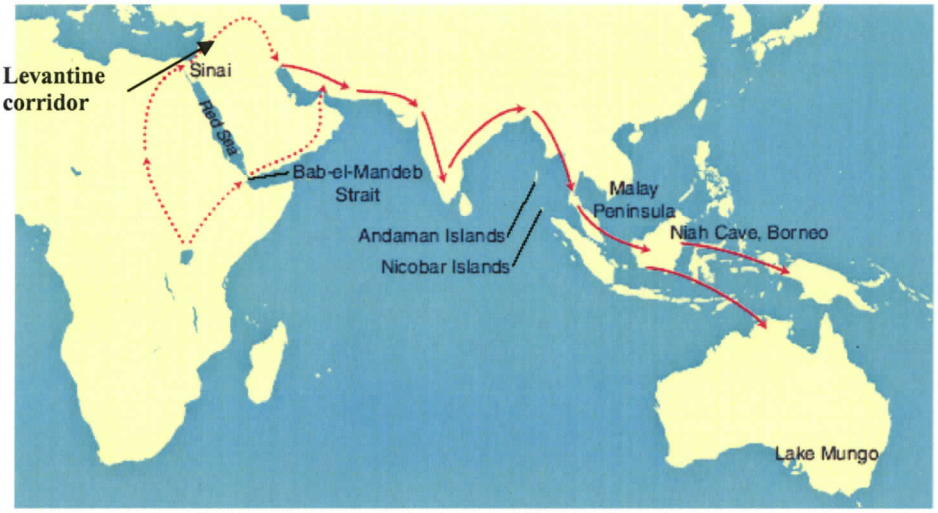

Figure 3: Hypothetical coastal and inland migration routes along the Indian Ocean coastline that have been proposed as possible routes taken by early Anatomically Modern Humans emigrating out of Africa (Forester and Matsumura, 2005)

Recently, support for the theories of a 'climate-driven migration' and a 'southern coastal migration' out of Africa for AMH has been derived from the discovery of a number of coastal sites along the eastern and southern coasts of Africa that suggest that a novel transition to coastal living occurred around 125 kya. The most infamous coastal site, dating back 125 kya, was in Abdur, along the Red Sea coast of Eritrea in East Africa. Embedded within this raised fossil reef researchers found broken fragments of oysters, giant clams and crustaceans, as well as fossils of terrestrial mammals such as elephant, hippopotamus, rhinoceros and bovid (species not determined) along with abundant stone tools (Walter et al., 2000). It appears that the humans who lived at the site may have driven some of those animals toward the sea and killed them there to supplement their seafood diet (Walter et al., 2000). Despite the fact that human fossils remains at this site have not yet been recovered, the date coincides with the apparent transition from archaic-to-modern *Homo sapiens* based on available fossil evidence from terrestrial sites of the East African interior such as Lake Eyasi (~130 kya), Mumba Rockshelter (~109 -130 kya), the Ngaloba beds (~120 kya) and Omo Kibish (~196 kya). The fossil evidence at these sites suggests that AMH were in East Africa by the time the reef site was forming, and thus being used by these coastal-dwelling humans (Walter et al., 2000). Evidence of this coastal adaptation by these humans is also supported by the sudden appearance of a number of South African coastal sites around the last interglacial-glacial transition (125 -75kya). These sites include the system of caves found at the

Die Kelders Cave 1 site dating back to 70 kya, the Blombos Cave site dating back to 70 kya, the Border cave site dating back to 100 kya and the Klasies River Mouth site dating back to 120 -115 kya (Singer & Wymer, 1982). At the Klasies River Mouth site (KRM), *Homo sapiens* fossils were found at dating 115 kya, and are perhaps the earliest known modern human remains (Singer & Wymer, 1982). There is also was evidence that the Klasies River cave people fished and harvested shellfish from the sea using some type of a boat. This scene was depicted in pictorials and impressions embedded in the rocks and sand (Singer & Wymer, 1982).

Presently, the Eritrea site and the KRM site are the earliest evidence of a human adaptation to seashore living (Walter et al., 2000), suggesting that there was a major change in human adaptive capacities at about this time. The attraction of coastal zones for early human occupation and dispersal lies in the fact they facilitate movement and provide more equable climates and diverse terrestrial and marine resources (Sauer, 1962). Guided by this archaeological evidence it has been argued, but not yet established, that movement along the coasts might have been in response to hyper-arid conditions and dwindling water resources inland caused by climatic stress. Based on new evidence in Eritrea, paleoclimatic data and fossil dates in Australia, a time window of 110-90 kya has been proposed for the migration of AMH from Africa towards Asia (Stringer, 2000; Walter et al., 2000). As a result of the apparent synchronicity between this early human migration event and the 'Last Glacial Cycle' the focus has been placed on quantifying how global climate and regional climate in Africa during this time may have influenced the geographical range dynamics of AMH. The following section of the study will examine the climate change that occurred in both Africa and the North Atlantic region between Marine Isotope Stage (MIS) 5e (125 kya) through MIS 4 (72 kya), as this is the time period that is relevant to this study.

4.0 Climate Change during the Last Glacial Cycle

4.1 The Global Pattern of Climate Change

In global terms, the Quaternary period is characterized by the alteration of cold glacial and warm interglacial periods. There were at least nine glacial-interglacial cycles between 2 and 0.7 Mya (Shackleton & Opdyke, 1973; Shackleton & Hall, 1984) with at least ten after that (Imbrie et al., 1984). In global terms, the Last Glacial Cycle (LGC) was the coolest and most variable of the Pleistocene with wide climatic fluctuations that occurred across a range of temporal and spatial scales. At the onset of the last interglacial (130 ka), atmospheric CO_2 and CH_4 levels were rising rapidly in association with an increase in globally averaged surface-air temperature (Finlayson, 2005). In the Northern Hemisphere, the LGC is characterized by the deglaciation that took place at the end of Marine Isotope Stage (MIS) 6 around 130 kya, followed by a brief interglacial during MIS 5e (128-120 kya) which ended around MIS 5d (117-115 kya), with the return of cold temperatures (glacial inception) and a subsequent gradual climatic deterioration at MIS 4 when the Earth reached full glacial conditions of the Pleistocene 'Ice Age' (72 -62 kya) (Imbrie et al., 1984).

Sea level was also higly variable in the Quaternary due to the growth and decay of the ice sheets. Sea level lowstands are associated with glaciations and highstands with interglacials. The global picture is of rapid rise in sea levels of the order of 20 m per 1 kyr to a highstand during MIS 5e with sea levels between 2 and 12 m above present (van Andel & Tzedakis, 1996). This was followed by a variable but progressive drop in sea levels to Last Glacial Maximum[5] lowstand between -118 and 135 m (Clark & Mix, 2000).

4.2 The African Pattern of Climate Change

The shift towards increased cooling and aridity is detected in Africa after 2.8 Mya (deMenocal, 1995). However, after 200 kya, African glacial stages were more arid than those of the middle Pleistocene (Jahns et al., 1998). The variability in the African landscape during the

[5] The Last Glacial Maximum refers to the time of maximum extent of the ice sheets during the last glaciation, approximately 21 kya

Quaternary has been proposed as a major factor influencing the dispersal of tropical African animals, including early humans (Finlayson, 2005). This section will review the paleoclimate data available for the African continent during the LGC.

North and West Africa

During LGC, paleoclimate studies indicate that the Africa climate began to shift towards colder and more arid conditions between 110-11 kya (Adams, 1997). Marine records of pollen and dust flux off the west coast of Africa indicate that around 125- 120 kya, during the moistest phase of the Eemian Interglacial (MIS 5e), rainforest occupied a far greater area than at present in West Africa, and rainfall was generally higher over North Africa (Frenzel, 1992; van Andel & Tzedakis, 1996). This respite of warmth lasted until about 115 kya (MIS 5d), when it appears that the north-western African environment gradually entered a phase of extreme aridity (van Andel & Tzedakis, 1996). Subsequent cooling and drying of the climate led to a cold maximum about 75 kya (van Andel & Tzedakis, 1996). In addition, detailed marine sediment records from Cap Blanc in north-western Africa have revealed that over the last 160 kyr (MIS 6), the pollen content and flux were lower during glacial periods and higher during the wet interglacial periods (Zhao et al., 2003). The lower pollen flux is mainly caused by the concomitant sparse vegetation cover on the northwest coast of the African continent (Zhao et al., 2003). The Sahara changed dramatically during this period. During the LGC the desert was even more extensive than it is today (Grove & Warren, 1968; Swezey, 2001). From 125-115 kya, the Saharan-Sahelian boundary shifted from a northern position at 23°N to as far south as 15° N; however during the rest of MIS 5, the Saharan-Sahelian boundary migrated back and forth between ca. 21°N –19 °N (Dupont and Hooghiemstra, 1989). In West Africa, rainforest was strongly reduced after 115 kya, especially during MIS 5d (115 -105 kya) and 5b (93 -85 kya) when *Montane*[6] forest, indicative of cool environments, expanded in its place (Dupont and Hooghiemstra, 1989). According to marine sediment cores retrieved off the Ivory Coast (Fredoux, 1994), the Niger Delta (Lutze et al., 1988) and off the coast of Gabon (Lutze et al., 1988), the *Podocarpus*[7] forest area strongly expanded during the cold stadials of the LGC in MIS 5d (115 to 105kya) and 5b (93 to 85 kya). A strong rise in the percentages of *Podocarpus*

[6] Type of coniferous forest, dominated by spruce. fir and pine trees

[7] *Podocarpus* is the genus ascribed to family of yellowwood, brown and black pine trees (evergreen shrubs or trees). These trees are moderately drought-resistant, frost hardy and grow best on moist mountainous areas and forests.

pollen suggests that the climate in West Africa became cooler, but remained humid (Dupont & Agwu, 1992).

East Africa and Arabia

Palynological evidence of the vegetation of northeast Africa and the Arabian Peninsula comes from a marine pollen record from the Arabian Sea (Van Campo et al., 1982). The record shows marked high relative amounts of pollen from the Sudanian savannah and humid tropical taxa signalling a strong southwest monsoon during the last Interglacial (MIS 5e). During the glacial periods, relative amounts of pollen from the Mediterranean *steppe*[8] increase and the humid tropical taxa decrease indicating a shift of the main pollen source area from East Africa to the Arabian Peninsula (Van Campo et al., 1982). Dust transport into the Arabian Sea reconstructed from the western Arabian Sea (Leuschner et al., 2004) and the northern Arabian Sea (Reichart et al., 1998) has revealed that during the warm MIS 5c (105 -93 kya) and 5a (85 -75), dust deposition from the Arabian Peninsula was greatly reduced, which implies more humid conditions there. In contrast, during the cold MIS 5d (115 -105 kya), 5b (93-85 kya), and 4 (75 -60 kya), and the LGM (18 -10 kya), large quantities of dust were deposited in this area.

Southern Africa

There are indications from the record of desert-dune formation across the Kalahari Desert in southwestern Africa that between 90-110 kya (MIS 5d - 5b) Africa became extremely arid (Stokes et al. 1997). These records indicate that Africa experienced extreme dune-building (arid) phases at ~115 -95 kya, 41 -46 kya, 26 -20 kya and 16 -9 kya (Stokes et al., 1997). These 'active' depositional phases were presumably punctuated by more humid periods during which time rainfall was greater (Stokes et al., 1997). Central to the paleoclimatic interpretations of Stokes et al., (1997) is the assumption that these past changes in aeolian dynamism must be related to changes in rainfall intensity in the area, and thus must represent periods of increased aridity.

The significance of these changes is that the climatic variability of the late Pleistocene produced a large-scale temporal and spatial scenario of changing habitats, landscapes and barriers

[8]Dry semi-desert vegetation that consists of drought tolerant shrub species like sage and grasses

that may have enabled or compelled African AMH to expand their geographical range and colonize Eurasia. By setting these records of regional environmental changes within the context of global climate change history, we are able to observe that in general, the dust fluxes were higher during glacial periods and lower during the wet interglacial periods, providing compelling support for the assertion that the development of arid conditions in Africa can be linked with high-latitude glacial-interglacial cycles. Furthermore, the investigation of the Pleistocene sediment retrieved from these deep sea cores provides an indication of the amounts of dust that have accumulated at different phases of the Quaternary and of vegetation changes that have taken place during this period.

5.0 The Link between Heinrich Events, Cold North Atlantic Sea Surface Temperatures and African Aridity during the late Pleistocene

Evidence from Greenland ice cores and pollen records from Europe show that the generally cold period of the LGC, between 115 and 14 kya, fluctuated repeatedly between periods of slow cooling (stadials) and relatively short periods of rapid warming (interstadials). A period of slow cooling followed by rapid warming is known as a Dansgaard-Oeschger (D/O) event (Bond et al.,1999; Dansgaard et al., 1989). Each successive D/O event results in warming that does not return to the greatest warmth of the previous cycle, and subsequently results in an even greater level of cooling than the previous D/O event (Bond et al., 1999). After a number of cooling/warming episodes there is a terminal dramatic cooling event, before the whole cycle happens again. Such a cycle of warming and cooling is known as a Bond Cycle (Bond et al.,1999; Dansgaard et al., 1989). The cold termination stage of a Bond Cycle coincides with the appearance, in ocean sediment cores, of extremely high lithic fragment, which are sediment fragments interpreted as having been carried by icebergs as they drifted into the North Atlantic Ocean. Therefore, the layers of sediment that mark the terminus of a Bond Cycle are considered to consist of Ice Rafted Debris (IRD) and are known as Heinrich layers (Bond et al.,1999, Heinrich, 1988) . The terminal phase of a Bond Cycle is therefore known as a Heinrich Event (HE), which is associated with short-lived but massive discharge of icebergs from the circum-Atlantic ice sheets (the Laurentide, Greenland, Iceland, Scandinavian, Barents Sea Ice sheets) that expanded over North America and Europe during the LGC (Chapman and Shackleton, 1998). Over the last 150 kyr these HE occurred every 7 -13 kyr (every 5 or 6 D/O events), lasting 100 -500 years (Dowdeswell et al., 1995). The associated calving of the ice sheets during these HE resulted in the input of large volumes of freshwater in the North Atlantic, causing profound changes in sea surface conditions. Surface water paleoclimate records from the North Atlantic have shown that over the last 150 kyr, cold SSTs in the North Atlantic have been associated with the occurrence of HE (Dowdeswell et al., 1995). See Figure 4 to view the modern path of the North Atlantic Current (NAC) that carries warm and salty water from the tropics to the North Atlantic region and the main belt of iceberg discharge (area shaded in grey).

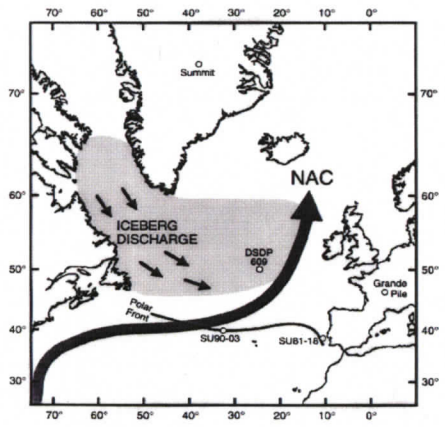

Figure 4: The modern path of the North Atlantic Current (NAC) and the main belt of IRD accumulation (area shaded in grey). Chapman and Shackleton, 1998

It is generally accepted that much of the observed surface temperature variability in the North Atlantic over the last 150 kyr was due to significant changes of the global ocean THC, induced by freshwater discharge into the North Atlantic during these HE (Clarke & Prairie, 2001; Broecker, 1997). The global ocean THC has a unique circulation pattern; the northeast trending Gulf Stream carries warm and relatively salty surface water from the Gulf of Mexico up to the seas between Greenland, Iceland and Norway (Gagosian, 2003). Upon reaching there, the ocean gradually releases its heat to the atmosphere, acting as a massive "central heating system" for Europe and land downwind (Rahmstorf, 2003). As the surface water cooled off and (with the combination of being cooler and relatively salty) becomes dense enough to sink into the deep ocean it forms the water mass known as North Atlantic Deep Water (NADW). As the NADW sinks it is theorized that it exerts a 'pull' that helps maintain not only the strength of the northward-moving warm Gulf Stream, but also the larger global ocean circulation (Rahmstorf, 2003). Based on deep-sea sediment and ice core records from the North Atlantic, the THC has slowed and shut down several times in the past, curtailing heat delivery to the North Atlantic and causing substantial cooling throughout the North Atlantic region (Rahmstorf, 2003; Fanning and Weaver, 1997). Several dynamical ocean models indicate that an influx of fresh water into the North Atlantic's surface could create this break in flow by decreasing the salinity of the water and the formation of NADW (Rahmstorf, 2003; Fanning and Weaver, 1997).

Over the years several HE have been documented in North Atlantic marine sediment records. Following the initial decay of ice sheets that had grown during the penultimate glaciation HE 11 occurred around 128 kya, a period of increased iceberg melt water and debris discharge in the North Atlantic (McManus et al., 2002). It was associated with surface water freshening and cooling (McManus et al., 2002). By mid sub-stage 5e (120 kya), regional SSTs were near modern values (CLIMAP, 1984; Chapman and Shackleton, 1998). As ice sheets began to grow, the region generally stayed warm. Only late in the ice sheet growth cycle did the entire sub-polar North Atlantic cool significantly, labelled by McManus et al (2002) as cooling event 24 (C24), which peaked at around 107 kya (within MIS 5d). This cooling event influenced the entire region, with much of the sub-polar ocean undergoing a cooling on the order of 4°C (McIntyre et al., 1976). Another warming followed, beginning within MIS 5d, and was followed in turn by the cooling event C23 at ~102 -103 kya. The warm interval corresponds to Greenland interstadial 24 (Dansgaard et al., 1993). In the Nordic Sea, C24 event was associated with an increase in IRD input; however, widespread ice rafting does not appear to have affected the mid-latitude North Atlantic until later during Heinrich event 9 (~105 kya) (McManus et al. 1994). Eight other ice-rafting events, labelled HE 1 –HE 8, have been identified in North Atlantic marine sediment records dating between 90 – 16 kya (Heinrich, 1988; Broecker, 1994; Bond and Lotti, 1995). However, the HE that occurred in closest proximity to the 100 kya-mark, assigned to the migration of AMH out of Africa, was HE 9.

5.1 Global Imprint of Heinrich and Dansgaard-Oeschger Events

Rapid changes in ocean and atmosphere circulation, induced by HE and D/O events, have been linked to abrupt climate change in tropical/ subtropical areas. The pollen record in Florida's Lake Tulane reveals alternating pine and oak episodes geared to the Heinrich-event timing (Grimm et al., 1993). A sediment core from Brazil's continental margin shows a large pulse of continental debris for each HE (Arz et al., 1998). A Chinese loess record shows intensified winter monsoons that correlate with HE (Porter and An, 1995). A sediment record from the Arabian Sea off Pakistan shows both D/O and HE (Schulz et al., 1998). Detailed analysis of the species abundances of planktonic foraminifera assemblages from a sedimentary sequence drilled in the Alboran Sea in the western Mediterranean has provided convincing evidence that during HE, SSTs and land surface temperatures in the western Mediterranean were considerably colder (Cacho et al., 1999). This

theory was reinforced by Arz et al (2001) who presented new results from an equatorial Atlantic core from beneath Africa's bulge showing that HE were associated with dry episodes in Africa (Arz et al., 2001). In Figure 5 (below) the sites where these studies show the climatic impacts of HE dominate are indicated with blue dots; sites where those of D/O events dominate are indicated with red dots. The black arrow shows the pathway followed by the ice surges. Accordingly, arid conditions prevail when North Atlantic SSTs are relatively cool and the South Atlantic is warm.

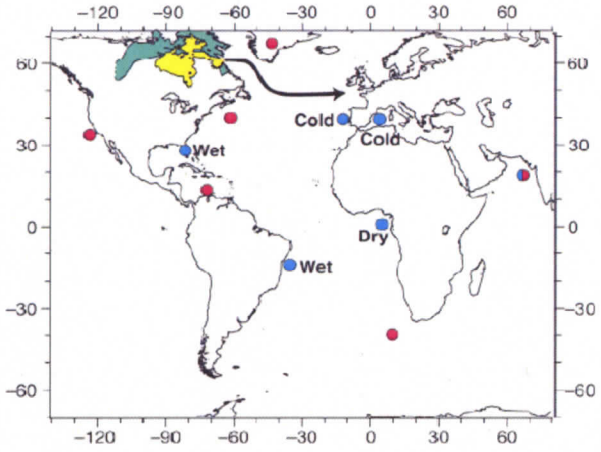

Figure 5: Spatial patterns of climate change events. Based on the compilation of studies by Grimm et al., 1993; Patzold and Wefer, 1988; Porter and An, 1995; Schulz et al., 1998; Cacho et al., 1999; Arz et al., 2001

Moreover, using pollen data researchers have discovered that a rapid transition from a green Sahara to today's desert conditions occurred around 5,700 years BP(Elenga et al., 2000). During the same time period, deMenocal et al (2000) found that ocean temperatures in the subtropical Atlantic Ocean, off western Africa, dropped around 5° C between 5,700-5,000 years BP, and that there was a dramatic increase in the amount of dust in the marine sediment records collected off the western margins of the African continent. At the same time, Oppo et al (2003) found a downward trend in North Atlantic Deep Water production around 6,500 years BP and ending around 5,000 years BP. This also occurred in tandem with a period of greater freshwater flux to the North Atlantic (Bond et al., 2001). Based on these results a large body of research has

been devoted to identifying the role that North Atlantic SSTs played in modulating African climate, and the contraction and expansion of African vegetation biome

5.2 The Response of the African Monsoon and the Intertropical Convergence Zone to Cold North Atlantic Sea Surface Temperatures

The extreme seasonal range in North, West and Central Africa rainfall is a consequence of the seasonal migration of the intertropical convergence zone (ITCZ) and the monsoon cycles. The Intertropical Convergence Zone (ITCZ) is an area of low pressure that forms where the northeast trade winds meet the southeast trade winds near the earth's equator. As these winds converge, moist air is forced upward, which favors the formation of heavy thunderstorms. The ITCZ is one of the dominant controls on precipitation patterns in the Atlantic region (as well as the rest of the tropics) (Dahl et al., 2005). This band moves seasonally over land, always being drawn toward the area of most intense solar heating, or warmest surface temperatures. However, the ITCZ is less mobile over the oceanic longitudes, where it holds a stationary position just north of the equator.

During the Northern Hemisphere (NH) summer, (when the sun is directly overhead in the NH) sensible heating over the North African land surface creates a low-pressure system over West-Central North Africa, drawing moist maritime air from the southwestern tropical Atlantic into western and central subtropical Africa (Hastenrath, 1985), creating a wet summer monsoon season (African Monsoon). East African summer rainfall is also related to the westerly airstream of the African monsoon, but is highly variable due in part to topographic rainshadow effects (Nicholson, 1993). During the NH summer, warm moist winds also blow from the southeast from the Indian Ocean during the Indian Monsoon, usually bringing much needed rainfall to the Sahara, the Horn of Africa and the Arabian Peninsula (Wilson & Henderson-Sellers, 1985). In addition, during the NH summer strong southeast tradewinds dominate, and as a result of intense sensible heating over the North African land surface the ITCZ and its associated rain belt moves further north of the equator, causing heavy rainfall over the Sahel region.

In contrast, during the NH winter (when the sun is directly overhead in the SH), the African and Asian landmasses cool relative to adjacent oceans and the regional atmospheric circulation reverses; a high-pressure system develops in northwest Sahara Desert causing cold denser air to

develop over the African continent resulting in an outward flow of air from the continent from the dominating northeast trade winds. The dry northeast trade winds inhibit precipitation (Wilson & Henderson-Sellers, 1985) and due to the cooling of the North African landscape the ITCZ, and its associated rain belt, moves southwards and closer to the equator. As a result drought conditions persist in the Sahel region.

The ITCZ is sensitive to changes in the tropical SSTs. The colder-than-normal SSTs in the northern tropical Atlantic create a SST difference between the Northern and Southern Hemispheres (the SST gradient), which in turn generates a north-south surface pressure gradient in the atmosphere and a northerly wind anomaly near the equator (Chang, 1998). As a result the ITCZ and its associated rainfall belt moves farther south of the equator than normal, creating persistent drought conditions in the Sahel Region (Chang, 1998). In theory, we can postulate that if North Atlantic SSTs remained cold for an extended period of time, the seasonal migration of the African monsoon and the ITCZ could have been attenuated, thus allowing dry, arid conditions to prevail in the subtropical Africa during these cold SST events.

6.0 Climate Model Description and Experimental Design

6.1 Description of the University of Victoria Earth System Climate Model

The experiments conducted in this study use version 2.7 of the intermediate complexity University of Victoria Earth System Climate Model (UVic ESCM) (Weaver et al., 2001). The UVic ESCM consists of a three-dimensional ocean general circulation model (Pacanowski, 1995) coupled to a thermodynamic/ dynamic sea-ice model (Hibler, 1979; Hunke and Dukowicz, 1997), an energy-moisture balance atmospheric model with dynamical feedbacks (Fanning and Weaver, 1996), and a thermo-mechanical land-ice model. The reduced complexity atmosphere model, developed by Fanning and Weaver (1996), is used for computational efficiency. The model is global in coverage and each component in the model has a spherical grid resolution of 3.6° (zonal) and a meridional resolution of 1.8°.

The atmospheric component of the model is based on Fanning and Weaver (1996) energy-moisture balance model. Some major simplifications to the atmosphere model are the formulation of the vertically-integrated thermodynamic energy balance equations, which assume an exponentially decreasing vertical distribution of energy and humidity (from surface values) with specified e-folding scale heights. Other major simplifications include the fact that momentum conservation equations are replaced by specified wind data, and the atmospheric heat transport is parameterized through Fickian diffusion and moisture transport is achieved through advection and diffusion. Precipitation is assumed to occur when the relative humidity is greater than 90%, and precipitation, which falls as rain over land is assumed to return instantaneously to the ocean via one of 33 observed river drainage basins. Precipitation falls as snow when surface atmospheric temperatures decrease below -5°C. The model is driven by a full annual cycle of incoming solar radiation at the top of the atmosphere, which is controlled by the orbital parameters: eccentricity, obliquity and precession of the equinoxes (Berger, 1978), which enable the model to be used in both equilibrium paleoclimate applications and long transient paleoclimate integrations.

The ocean and ice components of the coupled model are also forced by a monthly wind stress climatology, created from 40 years (1958-1998) of daily NCEP reanalysis data of Kalnay et al., (1996), and thus the model is integrated to equilibrium with specified present-day winds. Ice

and snow albedo feedbacks are included in the coupled model by locally changing the surface albedo. The atmospheric model includes a parameterization of water vapour/ planetary long-wave feedbacks, although the radiative forcing associated with changes in atmospheric CO_2 is included as a modification of planetary long wave radiative flux. A specified lapse rate is used to reduce the surface temperature over land where there is topography.

The dynamic global vegetation model called 'TRIFFID' (Top-down Representation of Interactive Foliage and Flora Including Dynamics) was developed at the Hadley Centre (Cox, 2001) and is coupled to the UVic ESCM. TRIFFID defines the state of the terrestrial biosphere in terms of soil carbon, and the structure and coverage of five plant functional types (PFT): broadleaf trees, needleleaf trees, C4 Grass, C3 Grass, shrub trees, as well as barren soil. The five vegetation types are represented as a fractional coverage in each grid cell, and compete amongst each other for the dominance as a function of the model simulated climate. Competition between natural PFTs is based on a tree-shrub-grass dominance hierarchy, with dominating types limiting the expansion of subdominant types, but not vice-versa. However, the tree types (broadleaf and needleaf) and grass types (C3 and C4) co-compete with competition coefficients dependant on their relative heights. Surface albedo is calculated interactively as a function of vegetation distributions, leaf area index and snow cover. The land surface model used to support the TRIFFID dynamic vegetation model is a single soil-layer version of the MET Office Surface Exchange Scheme (MOSES) (Cox et al., 1999). The simplified MOSES land surface scheme is coupled to the UVic ESCM, and is used here to calculate soil moisture, soil, evapo-transpiration, surface and skin temperatures for each vegetation type and lying snow based on a single soil layer model of uniform 1-m thickness as described by Meissner et al., (2003). MOSES and TRIFFID calculate terrestrial carbon stores and fluxes. The uptake of carbon in plant growth is defined as gross primary productivity and is a function of atmospheric carbon dioxide, solar radiation, soil moisture, humidity, leaf area index and temperature. The photosynthesis model used here is based on the leaf-level photosynthesis models for C3 and C4 grass of Collatz et al (1991, 1992). The resulting rates of photosynthesis and plant respiration are dependant on both atmospheric carbon dioxide concentrations and climate conditions, determine the distribution of vegetation in the model and the response of vegetation to climate changes.

The ocean component of the coupled model is based on the Geophysical Fluid Dynamics Laboratory Modular Ocean Model (MOM) 2.2, with a global resolution of 3.6° (zonal) by 1.8° (meridional) and 19 vertical levels, and includes an option for brine-rejection parameterization. Mixing associated with mesoscale eddies is prescribed according to Gent and Williams (1990). The ocean model also uses a constant salt-to-freshwater mass ratio of $3.49 * 10^{-2}$ to convert surface freshwater fluxes to fluxes of salt. The sea-ice component of the model is represented by a relatively simple zero layer formulation of Semtner (1976), which includes parameterization for both lateral growth and melt based on the parameterization of Hibler (1979). The model generates ice thickness, areal fraction of ice and ice surface temperature. The sea-ice component consists of an elastic-viscous-plastic rhealogy to represent sea-ice dynamics.

The present-day (PD) model simulation was integrated to equilibrium with orbital, CO_2, ice sheet elevation and ice sheet areal extent forcing specified for the year 1850. This was the PD climate simulation used to compare with the results of the experiments conducted in this study (control run), in order to identify and quantify the observed changes from present-day climate. The UVic ESCM has been extensively and successfully used in a wide range of scientific experiments involving both contemporary and paleoclimates, and the systematic comparison of the coupled model with contemporary climate and paleoclimate observation reveals good agreement.

6.2 Experimental Design

To explore the climate processes potentially responsible for promoting hyper-arid conditions in Africa during the late Pleistocene, especially around 100 kya, I used the UVic ESCM to conduct two climate model experiments. The first experiment, referred to here as '105K2 simulation', involved simulating a global climate system that corresponded to 105 kya by prescribing an orbital insolation configuration as documented by Berger (1978), and atmospheric CO_2 forcing appropriate for 105 kya as documented by Petit et al (1999). For the purpose of this study, I chose to simulate climate at this time interval because the second experiment involved simulating HE 9, which is documented to have occurred 105 kya (Heinrich, 1988; McManus et al., 1994). The objective of experiment two, referred to here as the 'FW105C2 simulation', was to simulate an actual HE that occurred closest to the100 kya-mark assigned to the migration event of AMH, in order to test whether HE played a role in the aridification of Africa around 100 kya. In

order to simulate a Heinrich 9-like (HE 9-like) climate state, I used the 105K2 simulation (105 kya-like climate state) as my initial conditions and applied a freshwater flux to the northern North Atlantic region of the model. The climate anomalies associated with both the 105K2 and the FW105C2 simulation were derived from comparing the results of each simulation to the simulation of present-day climate labelled here 'PD'. Subsequently, the climate anomalies of both experiments (difference from PD) were contrasted with each other. The 105K2 and FW105C2 simulations were compared to a simulation of present-day climate, rather than a simulation of climate corresponding to the last warm interglacial period (~125 kya), due to the fact that the both simulations were initiated from a model simulations of present-day climate and subsequently forced under 105 kya orbital parameters, atmospheric carbon dioxide levels and fresh water influxes. Furthermore, although the systematic comparison of the UVic ESCM with contemporary climate and paleoclimate observation has revealed good agreement, the most common method used to evaluate climate models involves comparing the model results with present-day climate simulations, as there exists a wide range of climatological present-day observations to evaluate it against. Therefore, in order to ensure the validity of the results and a clean comparison of the results of this study, the model results of the two experiments were compared with the simulation of present-day climate, from which they were initialized from. It should also be noted that based on paleoclimate datasets dating back 125 kya it is thought, but not yet established, that the last interglacial period was at least as warm as the present climate (Felis et al., 2004). See Table 1 for the orbital configurations, atmospheric CO_2 concentrations and freshwater influx rate used in each experiment.

6.2.1 Orbital and Atmospheric Carbon Dioxide Forcing Experiment (105K2)

The '105K2' simulation was initialized from an equilibrium model of climate at 115 kya. The 115 kya simulation was originally created by forcing a model simulation of the Earth's present-day climate (PD) with an orbital configuration that corresponds to 115 kya, as documented by Berger (1978), whereas the atmospheric CO_2 concentration was kept constant at 280 ppmv (pre-industrial values, yr 1850). The simulated climate for 115 kya was then forced with orbital parameters and atmospheric CO_2 levels appropriate for 110kya. This 110 kya simulation was run for 3000 yrs in order to reach a quasi-equilibrium state. Once the 110 kya simulation reached a

quasi-equilibrium, I repeated this procedure, and forced the 110 kyr simulation equilibrium model run with both orbital configurations and atmospheric CO_2 concentrations corresponding 105 kya. This is the '105K2' model used here to represent the 105 kya-like climate state. See Table 2 for the orbital configurations and CO_2 concentrations used.

6.2.2 Orbital, CO_2 and Freshwater Forcing Experiment (FW105C2)

To simulate a climate evolution, which could be considered to be representative of HE 9, I applied a surface freshwater flux with an amplitude of 0.1 Sv (1 Sv= $10^6 m^3 s^{-1}$) to the northern North Atlantic region of the model (between 50°N and 75°N) for 300 years, using the 105K2 simulation as my initial conditions. At the end of the 300 year period, the freshwater flux was turned off, and the model was run for another 2700 years to allow it to reach a quasi equilibrium state. The 300 yr duration of the freshwater influx compares favorably with the Dowdeswell et al. (1995) interpretation of the North Atlantic marine sediment record which suggests that HE last 100 -500 kyr. In addition, the rate of 0.1 Sv is comparable to estimates of glacial melt-water (Licciardi et al., 1999) and ice-rafted debris (MacAyeal, 1993) inputs into the North Atlantic during the Younger Dryas. Thus, the results of this experiment are a combination of applying an orbital configuration and atmospheric CO_2 values appropriate for 105 kya, in addition to the freshwater flux perturbation applied into the northern North Atlantic region. It should be noted that this study does not model iceberg drift and melting; rather it simulates the consequences of the iceberg melt water by prescribing its impact on sea surface salinity. It should also be noted that this study did not account for a drop in sea level. This was not included in order to have a clean comparison with the present-day integrations.

The orbital configuration at 105 kya is characterized by both a smaller obliquity, a larger eccentricity and a smaller perihelion than today, as specified by Berger (1978) (Table 1). The small obliquity reduces seasonality, i.e. less insolation at high-latitudes in both hemispheres during their respective summers (cool summers) and more insolation in their winters (warm winters). However, the effect of the smaller obliquity is counteracted by the smaller precession at 105 kya, which enhances the seasonality in the Northern Hemisphere (NH) and reduces seasonality in the Southern Hemisphere (SH), i.e. more insolation in the NH summer (warm summers) and less insolation in

the NH winter (cold winters), while it causes less insolation in the SH summer (cool summers) and more insolation in the SH winter (warm winters). The impact of the precession at 105 kya is intensified by the larger eccentricity, which decreases the distance between the sun and the perihelion, while it increases the distance between the sun and the aphelion. Overall, under this orbital configuration there would more seasonal contrast in the NH (warm summer and cold winter) and less seasonal contrast in the SH (cool summer and warm winters) 105 kya.

In nature, and in the UVic ESCM, the warmer NH summer would have resulted in a stronger summer African monsoon (wetter conditions in subtropical Africa) and stronger southwest (Indian) monsoon (wetter conditions in Sahara, the Horn of Africa and the Arabian Peninsula). In addition, the colder NH winter would have resulted in a stronger winter African monsoon (drier conditions in subtropical Africa) and stronger winter Indian (southwest) monsoon drier conditions on the Indian continent). However, counterintuitive to what these results would lead one to expect, the intense precipitation in the summer and the intense drying during the winter in Africa do not cancel each other out because it is the intensity of the summer monsoon that determines the annual amount of rainfall. Therefore, we would expect subtropical Africa to receive more moisture at 105kya due to the orbital configuration. In addition, the atmospheric CO_2 concentration at 105 kya is also characterized by lower CO_2 levels than today. A fixed CO_2 concentration of 230 ppmv is used for both the 105K2 and FW105C2 experiment, whereas a fixed CO_2 concentration of 280 ppmv (pre-industrial levels) was used for the present-day simulation (PD), as specified by Petit et al., (1999). The results of Petit et al (1999) were used in this study, as these results allowed this study to include the effect of small variations atmospheric CO_2 of approximately 20–30 ppmv reconstructed for stadial-interstadial changes. As previously stated, the reduced atmospheric CO_2 would directly cool the atmosphere. It should be noted that the climate anomalies defined for each analyzed region were estimates of annual mean climate anomalies. It should also be noted that these types of simulations are clearly idealized sensitivity experiments and cannot be viewed as a precise attempt at simulating the past.

Table 1: Description of atmospheric Carbon Dioxide (CO_2), Orbital Parameters (Perihelion, Obliquity and Eccentricity) and Freshwater Flux Rate (FW) Forcing applied to the 105K2, FW105C2 and PD simulations

Name of Experiment	CO_2 (ppmv)	FW (Sv)	Perihelion (°)	Obliquity (°)	Eccentricity
PD	280.00	0.00	283.00	23.44	0.02
105K2	230.00	0.00	98.34	22.97	0.04
FW105C2	230.00	0.10	98.34	22.97	0.04

Table 2: Description of atmospheric Carbon Dioxide (CO_2) and Orbital Parameters (Perihelion, Obliquity and Eccentricity) used to generate the 105K2 climate simulation

Name of Simulation	CO_2 (ppmv)	Perihelion (°)	Obliquity (°)	Eccentricity
115kyr	280.00	289.21	22.41	0.04
110kyr	250.00	15.49	22.40	0.04
105kyr	230.00	98.34	22.97	0.04

7.0 MODEL RESULTS

The evaluation of this study's results is based on model simulations pertaining to the regions identified in the map in Figure 6. The regions analyzed in this study included: North Africa (Region 6), West Africa (Region 5), East Africa (Region 2), Central Africa (Region 4) and Southern Africa (Region 3). The purpose of dividing Africa into its five regions was to allow for the determination and comparison of the degree to which each region was impacted, and to facilitate the comparison of the model results with the paleoclimate data outlined in Section 4.1. The climatic variables analyzed in this study included: annual mean Surface Air Temperature (SAT), Evaporation (E), Precipitation (P), E minus P anomalies (E-P) and the Fraction Areal Coverage of the five plant functional types (FRAC) : Broadleaf trees (adapted to moist and warm climates), needleleaf trees (adapted to cold climates), C3 grass (adapted to humid climates), C4 grass (adapted to arid climates), shrub trees (adapted to arid climates), including barren soil (arid climates). While the primary focus was on the African climate, results from the subtropical and tropical Atlantic are also described because of the atmospheric teleconnections that link the subtropical and tropical Atlantic with the African monsoon. As a result this study also focused on the Atlantic Ocean, which was divided into two regions: the subtropical (23° N and 75° N, Region 8) and tropical (0° N and 23° N, Region 7) Atlantic Ocean basins (See Figure 6). The climatic variables analyzed in each region of the Atlantic included: annual mean Surface Air Temperature (SAT), Evaporation (E), Precipitation (P), E minus P anomalies (E-P), Sea Surface Temperature (SSTs), Sea Surface Salinity (SSS) and Meridional Overturning Circulation (MOC). The regional climate anomalies produced in the 105 kya-like climate state (105K2 experiment) and the HE 9-like climate state (FW105C2 experiment) were compared to the regional climate anomalies of the present-day climate state (PD or the control run), in order to assess the degree and direction of change, and contrast the cumulative effects simulated under each forcing regime.

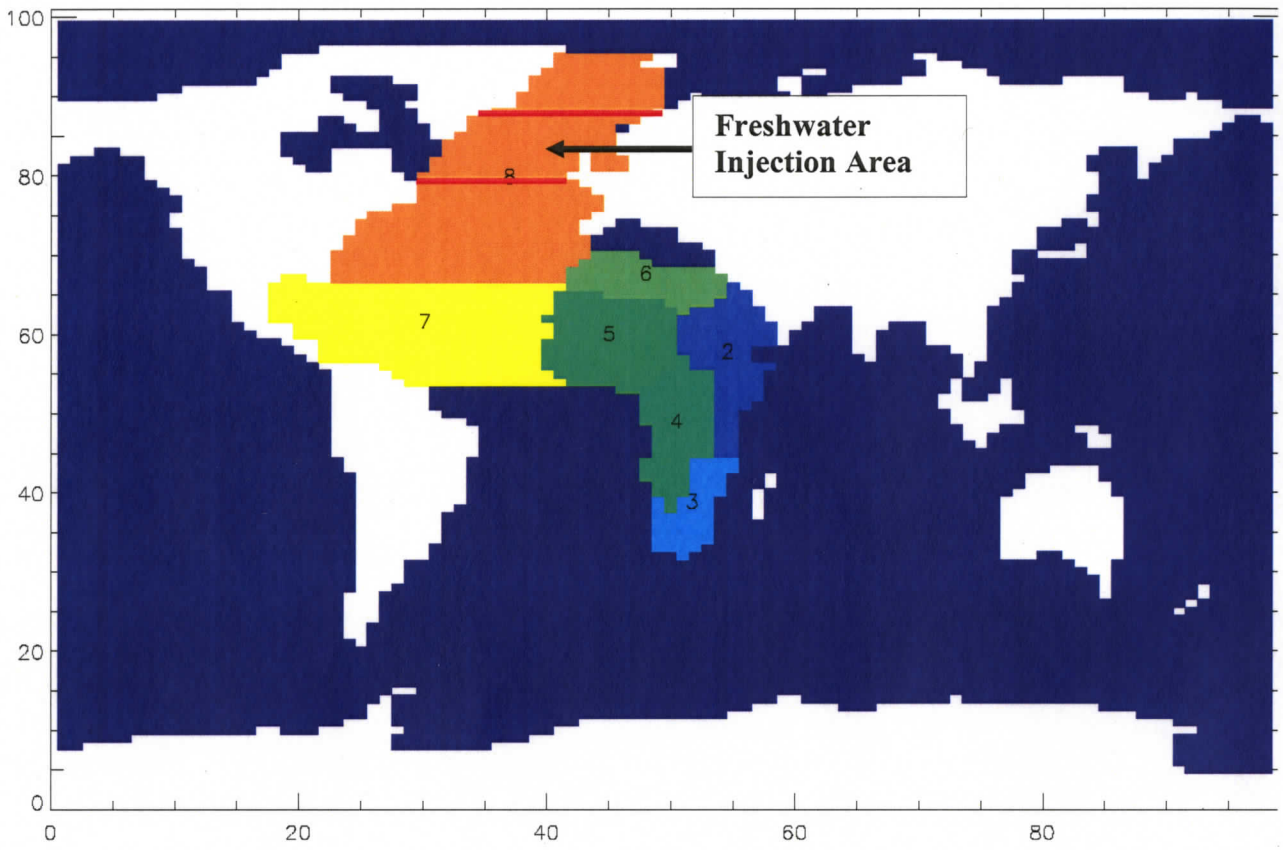

Figure 6: Regions in which climate anomalies were analyzed in this study. **2** East Africa, **3** Southern Africa, **4** Central Africa, **5** West Africa, **6** North Africa, **7** Tropical Atlantic, **8** Subtropical Atlantic

7.1 Atlantic Ocean Results

In Table 3, the maximum of the simulated annual mean meridional overturning circulation (MOC) in the Atlantic Ocean, associated with the THC, are shown for PD, 105K2 and FW105C2, as well as the differences between the 105K2 and FW105C2 simulations and PD (105k2 minus PD and FW105C2 minus PD). According to the results of the FW105C2 experiment, the injection of freshwater into the northern North Atlantic of the model led to a shut down of MOC in the Atlantic Ocean basin, as it was reduced by -19.2 Sv by the end of the freshwater pulse, relative to its PD rate. In contrast, the MOC in the 105K2 experiment increased by 1.1 Sv relative to its PD rate.

Table 3: Simulated Annual Mean Meridional Overturning Circulation (MOC) Anomalies for the Atlantic Ocean relative to present-day (PD) simulated in the 105K2 and FW105C2 simulations

Name of Model Output	MOC (Sv)
PD	19.2
105K2	20.3
FW105C2	0.0
105K2-PD	1.1
FW105C2-PD	-19.2

In Table 4 and 5 the subtropical and tropical Atlantic simulated climate anomalies for the annual mean Surface Air temperature (SAT), Precipitation (P), Evaporation (E), E minus P anomalies (E-P), Sea Surface Temperature (SSTs) and Sea Surface Salinity (SSS) are shown for PD, 105K2 and FW105C2, as well as the simulated differences in 105K2 minus PD and FW105C2 minus PD. Model simulations revealed that SSSs in the subtropical Atlantic were lower in both climate states relative to PD, although the reductions were significantly larger in the FW105C2 experiment (2.1 ppt lower than PD), as compared to the 105K2 experiment (0.2 ppt lower than PD). The same pattern was observed in the tropical Atlantic, in which the greatest reductions in SSSs occurred in the FW105C2 experiment (1.3 ppt lower than PD), as compared to the 105K2 experiment (0.1 ppt lower than PD). The reductions in SSSs in both regions of the Atlantic were accompanied by SST reductions relative to PD. In the subtropical Atlantic the greatest reductions occurred in the FW105C2 experiment (4.7 °C cooler than PD), as compared to the 105K2 experiment (1.9 °C cooler than PD). This cold SST anomaly was also observed in the tropical Atlantic, where the greatest reductions also occurred in the FW105C2 experiment (3.4 °C lower than PD), as compared to the 105K2 experiment (1.8 °C cooler than PD). From these results it is evident that although there were small reductions in SSSs and SSTs relative to today in the 105K2 experiment, it appears that the added freshwater flux played an amplifier role in the development of significantly colder SSTs and lower SSSs anomalies in the Atlantic Ocean at this time interval. This amplified affect can be attributed to the reduced MOC observed only in the FW105C2 experiment. As previously stated, the MOC in the Atlantic is sensitive to the freshwater budget at the sites of deepwater formation. In theory, the added freshwater flux to the North Atlantic in the

FW105C2 experiment decreased the formation of NADW, thereby reducing meridional heat transport, which caused cooling of the high-latitudes. This phenomenon will be further explained in the discussion section of this study (Section 8.0)

Table 4: Simulated Subtropical Atlantic Climate and Ocean Anomalies for the annual mean Surface Air Temperature (SAT), Precipitation (P), Evaporation (E) and E minus P anomalies (E-P), Sea Surface Temperatures (SST) and Sea Surface Salinity (SSS) simulated for the 105K2 and FW105C2 simulations relative to present-day (PD)

Name of Model Output	SAT (°C)	P (mm/a)	E (mm/a)	E-P (mm/a)	SST (°C)	SSS (ppt)
PD	10.8	1088.1	1166.7	78.7	12.4	34.9
105K2	8.2	1049.6	1096.6	47.0	10.5	34.7
FW105C2	4.7	888.1	833.1	-55.0	7.7	32.8
105K2-PD	-2.6	-38.5	-70.1	-31.7	-1.9	-0.2
FW105C2-PD	-6.1	-200.0	-333.6	-133.7	-4.7	-2.1

Table 5: Simulated Tropical Atlantic Climate and Ocean Anomalies for annual mean Surface Air Temperature (SAT), Precipitation (P), Evaporation (E) and E minus P anomalies (E-P), Sea Surface Temperatures (SST) and Sea Surface Salinity (SSS) simulated for the 105K2 and FW105C2 simulations relative to present-day (PD)

Name of Model Output	SAT (°C)	P (mm/a)	E (mm/a)	E-P (mm/a)	SST (°C)	SSS (ppt)
PD	23.1	1455.6	1734.8	279.2	24.2	35.6
105K2	21.0	1456.9	1699.9	243.0	22.4	35.5
FW105C2	19.2	1326.4	1609.3	282.9	20.8	34.3
105K2-PD	-2.1	1.3	-34.9	-36.2	-1.8	-0.1
FW105C2-PD	-3.9	-129.2	-125.5	3.7	-3.4	-1.3

In both the subtropical and tropical Atlantic, the reduction in annual mean SATs, SSTs and SSSs are accompanied by significant changes in both the annual mean precipitation (P) and evaporation (E) anomalies. In reference to Tables 4, in the case of the subtropical Atlantic there were reductions in P and E in both the 105K2 and FW105C2 experiments relative to today. However, the greatest reductions in P and E occurred in the FW105C2 experiment (200 mm/a or

18.0% less P and 333.6 mm/a or 28.5% less E relative to PD), as compared to the 105K2 experiment (38.5 mm/a or 3.5 % less P and 70.1 mm/a or 6.0% less E relative to PD). In the case of the tropical Atlantic (Table 5) the model simulations revealed that there was 1.3 mm/a or 0.1% more P and 34.9 mm/a or 2.0 % less E relative to PD in the 105K2 experiment, whereas in the FW105C2 experiment there were reductions in both P and E (129.2 mm/a or 8.9% less P and 125.5 mm/a or 7.2% less E than PD). Overall the E and P anomalies resulted in E minus P anomalies that suggest that the subtropical Atlantic was overall wetter than today in both the 105 kyr-like climate state and the HE 9-like climate state (P exceeded E), although it was 4 times wetter in the HE 9-like climate state. Furthermore, the E minus P anomalies for the tropical Atlantic suggest that the tropical Atlantic was slightly wetter in the 105kya-like climate state (P exceeded E), relative to PD, and slightly drier in the HE 9-like climate state than PD (E exceeded P).

7.2 African Climate and Vegetation Change Results

North Africa

In Table 6 below the simulated North African climate anomalies for annual mean Surface Air Temperature (SAT), Precipitation (P), Evaporation (E) and the E minus P anomalies (E-P) are shown for PD, 105K2 and FW105C2, as well as the simulated 105K2 minus PD and FW105C2 minus PD differences. As depicted in Table 6, the response of the model in both the 105K2 and FW105C2 simulations was a reduction in annual mean SAT in North Africa relative to today, although the greatest cooling occurred in the FW105C2 experiment (4.9 °C cooler than PD), as compared to the 105K2 experiment (2.6 °C lower than PD). The results also show that both the magnitude of the annual mean P and E anomalies for North Africa were lower in the FW105C2 experiment (1.3 mm/a or 0.5% more P and 3.5 mm/a or 1.3% less E than PD) than in the 105K2 experiment (101.9 mm/a or 35.0% more P and 82.2 mm/a or 30.0% more E than PD). The overall net impact of these E and P anomalies resulted in E minus P anomalies that suggest that North Africa was overall wetter than today in both 105 kya-like climate state and the HE 9-like climate state, although the E minus P anomalies suggest that North Africa was more moist in the 105 kya-like climate state, relative to the HE 9-like climate state. It should be noted that this outcome is due to the fact that the UVic ESCM presently over-estimates rainfall over North Africa due to the fact

that the areal coverage of the ITCZ band, parameterized in the model, is less narrow in the model than it is in nature. As a result the ITCZ, ands its rain belt, spreads further into North Africa than it should.

Table 6: Simulated North African Climate Anomalies for the annual mean Surface Air Temperature (SAT), Precipitation (P), Evaporation (E) and E minus P anomalies (E-P) simulated for the 105K2 and FW105C2 simulations relative to present-day (PD)

Name of Model Output	SAT (°C)	P (mm/a)	E (mm/a)	E-P (mm/a)
PD	15.5	287.3	266.1	-21.2
105K2	12.9	389.2	348.3	-40.9
FW105C2	10.6	288.6	262.6	-26.0
105K2-PD	-2.6	101.9	82.2	-19.7
FW105C2-PD	-4.9	1.3	-3.5	-4.8

In Table 7 the simulated fractional vegetative coverage anomalies for the five plant functional types, in addition to barren soil, in North Africa are shown for PD, 105K2 and FW105C2, as well as the simulated 105K2 minus PD and FW105C2 minus PD differences. Although there is no change in the areal coverage of broadleaf trees, needleleaf trees and shrub trees in North Africa, there are significant changes in the areal coverage of C3 grasses, C4 grasses and barren soil in both the 105K2 and FW105C2 simulations. As indicated in Table 7, the model results indicate that in the FW105C2 experiment the areal coverage of C3 grass was 8.1% lower than PD, as compared to being 3.1% lower than PD in the 105K2 experiment. Similarly, in the FW105C2 experiment the areal coverage of C4 grasses is 3.4 % lower than PD; as compared to being 0.1 % lower than PD in the 105K2 experiment. Model simulations suggest that the C3 and C4 grass coverage was replaced by barren soil in North Africa; however, the greatest expansion of barren soil occurred in the FW105C2 experiment there was 11.5 % more barren soil in North Africa relative to PD, as compared to 3.2 % expansion in the 105K2 simulation.

Table 7: Simulated Fractional Vegetative Coverage Anomalies (FRAC %) for the Five Plant Functional Types and Barren soil in North Africa simulated for the 105K2 and FW105C2 simulations relative to present-day (PD)

Name of Model Output	FRAC % Broadleaf	FRAC % Needleleaf	FRAC % C3	FRAC % C4	FRAC % Shrub	FRAC % Barren soil
PD	0.0%	0.0%	22.4%	14.6%	0.0%	63.0%
105K2	0.0%	0.0%	19.3%	14.5%	0.0%	66.2%
FW105C2	0.0%	0.0%	14.3%	11.2%	0.0%	74.5%
105K2-PD	0.0%	0.0%	-3.1%	-0.1%	0.0%	3.2%
FW105C2-PD	0.0%	0.0%	-8.1%	-3.4%	0.0%	11.5%

West Africa

In Table 8 the simulated West African climate anomalies for annual mean Surface Air Temperature (SAT), Precipitation (P), Evaporation (E) and the E minus P anomalies (E-P) are shown for PD, 105K2 and FW105C2, as well as the simulated 105K2 minus PD and FW105C2 minus PD differences. Similar to the results for North Africa, the largest reduction in annual mean SAT in West Africa occurred in the FW105C2 simulation (4.3 °C lower than PD), as compared to the 105K2 experiment (2.5 °C cooler than PD). Lower annual mean P anomalies also accompanied these SAT reductions, although the greatest reductions in P relative to PD occurred in the FW105C2 experiment (221.1 mm/a or 25.5% less P than PD), as compared to the 105K2 experiment (5.9 mm/a or 0.7% less P than PD). Model simulations showed that the annual mean E was lower than today in the FW105C2 experiment (20.9% or 161.7 mm/a less E than PD), as compared to the 105K2 experiment where E was higher than today (29.9 mm/a or 3.9 % more E than PD). Modeled E minus P anomalies for both the FW105C2 and the 105K2 simulations indicate that West Africa was drier in both the 105 kya -like climate state and the HE 9-like climate state relative to PD (E exceeded P), although the E minus P results indicate drying was more extensive in the HE 9-like climate state.

Table 8: Simulated West African Climate Anomalies for the annual mean Surface Air Temperature (SAT), Precipitation (P), Evaporation (E) and E minus P anomalies (E-P) simulated for the 105K2 and FW105C2 simulations relative to present-day (PD)

Name of Model Output	Sat (°C)	P (mm/a)	E (mm/a)	E-P (mm/a)
PD	20.1	865.4	772.9	-92.5
105K2	17.6	859.5	802.8	-56.7
FW105C2	15.8	644.3	611.2	-33.1
105K2-PD	-2.5	-5.9	29.9	35.8
FW105C2-PD	-4.3	-221.1	-161.7	59.4

In Table 9 the simulated fractional vegetative coverage anomalies for the five plant functional types, in addition to barren soil, in West Africa are shown for PD, 105K2 and FW105C2, as well as the simulated 105K2 minus PD and FW105C2 minus PD differences. In terms of vegetation, the greatest magnitude of vegetative change occurred in the HE 9-like climate state. According to the model results, broadleaf tree coverage in West Africa was reduced in both the 105K2 and FW105C2 experiments, although the greatest reduction occurred in the FW105C2 experiment (30.3% less than PD), as compared to the 105K2 experiment (20.6% less than PD). There were also reductions in the C3 grass and shrub tree coverage in both the 105K2 and FW105C2 experiment; however the reduction are negligible in the 105K2 experiment (1.1% less C3 trees and 0.1 % less shrub trees, relative to PD), whereas the reductions are small but significant in the FW105C2 experiment (6.0 % less C3 grass coverage and 8.0 % less shrub vegetation than PD). In contrast, model simulations show that the areal coverage of needleleaf trees, C4 grasses and barren soil expanded in both the 105K2 and FW105C2 simulations, although the greatest expansions occur in the HE 9-like climate state. Model simulations show that there were 18.3 % more needleleaf trees, 10.0% more C4 grasses and 16.2 % more barren soil than today in the FW105C2 experiment, as compared to the 105K2 simulation where there were 11.3 % more needleleaf trees, 9.8 % more C4 grasses and 0.9 % more barren soil coverage than PD. In West Africa, it is evident that under both forcing regimes there are reductions in the areal coverage of broadleaf trees, C3 grasses and shrub trees, which are compensated for expansions in needleleaf trees, C4 grasses and barren soil. However, the largest expansions and contractions of these specified plant types occurred in the HE 9-like climate state.

Table 9: Simulated Fractional Vegetative Coverage Anomalies (FRAC %) for the Five Plant Functional Types and Barren soil in West Africa simulated for the 105K2 and FW105C2 simulations relative to present-day (PD)

Name of Model Output	FRAC % Broadleaf	FRAC % Needleleaf	FRAC % C3	FRAC % C4	FRAC % Shrub	FRAC % Barren soil
PD	34.7%	0.8%	18.0%	12.0%	14.4%	20.0%
105K2	14.1%	12.1%	16.9%	21.8%	14.3%	20.9%
FW105C2	4.4%	19.1%	12.0%	22.0%	6.4%	36.2%
105K2-PD	-20.6%	11.3%	-1.1%	9.8%	-0.1%	0.9%
FW105C2-PD	-30.3%	18.3%	-6.0%	10.0%	-8.0%	16.2%

East Africa

In Table 10 the simulated East African climate anomalies for the annual mean Surface Air Temperature (SAT), Precipitation (P), Evaporation (E) and the E minus P anomalies (E-P) are shown for PD, 105K2 and FW105C2, as well as the simulated 105K2 minus PD and FW105C2 minus PD differences. Similar to the previous regions, the largest reduction in annual mean SAT in East Africa occurred in the FW105C2 experiment (3.9 °C lower than PD), as compared to the 105K2 experiment (2.7 °C cooler than PD). However, the magnitudes of these cold SAT anomalies are much smaller than the SAT anomalies in North and West Africa. As in North Africa, the East African simulations show that both the annual mean P and E anomalies were lower in the FW105C2 experiment (74.7 mm/a or 9.3% less P and 26.0 mm/a or 3.8% less E than PD), whereas in the 105K2 experiment the annual mean P and E anomalies were higher than today (21 mm/a or 2.6% more P and 50.1 mm/a or 7.3% more E than PD). However, the E minus P anomalies suggest an overall drying in East Africa relative to PD, in both the 105 kya-like climate state and the HE 9-like climate state, although drying was more extensive in the HE 9-like climate state.

Table 10: Simulated East African Climate Anomalies for the annual mean Surface Air Temperature (SAT), Precipitation (P), Evaporation (E) and E minus P anomalies (E-P) simulated for the 105K2 and FW105C2 simulations relative to present-day (PD)

Name of Model Output	Sat (°C)	P (mm/a)	E (mm/a)	E-P (mm/a)
PD	19.0	800.7	687.0	-113.7
105K2	16.3	821.7	737.1	-84.6
FW105C2	15.1	726.0	661.0	-65.0
105C2-PD	-2.7	21.0	50.1	29.1
FW105C2-PD	-3.9	-74.7	-26.0	48.7

As illustrated in Table 11 the broadleaf tree and the shrub tree coverage was reduced in both the FW105C2 (29.0% less broadleaf trees and 1.8% less shrubs than PD) and 105K2 (16.9 % less broadleaf trees and 0.2% less shrub trees than PD) simulations. The model results also show that in both the 105K2 and FW105C2 simulations there were expansions in needleleaf trees, C3 and C4 grasses and barren soil, relative to PD. The increases in the needleleaf tree coverage, relative to PD in the FW105C2 simulation (6.2% more) was significantly larger than the increases in the 105K2 simulation (0.3 % more). For C3 grasses the model results indicate that there was 15.8 % more C3 grasses than PD in the FW105C2, as compared to the 10.0% increase in the 105K2 experiment, relative to PD. The areal coverage of C4 plants is about 6.0 % more than PD in both the 105K2 and FW105C2 simulations. These changes are accompanied by 2.7 % more barren soil than PD in the FW105C2 simulation, as compared to the 0.3% expansion in the 105K2 simulation. Similar to North African simulation, although the direction of change relative to PD for these plant types is the same between the 105K2 and FW105C2 experiments, the magnitude of the change is overall greater in the HE 9-like climate state. The only exception is the simulated areal coverage of C4 grasses, in which the expansion, relative to today, is 0.4% greater in the 105K2 simulation.

Table 11: Simulated Fractional Vegetative Coverage Anomalies (FRAC %) for the Five Plant Functional Types and Barren soil in East Africa for the 105K2 and FW105C2 simulations relative to present-day (PD)

Name of Model Output	FRAC % Broadleaf	FRAC % Needleleaf	FRAC % C3	FRAC % C4	FRAC % Shrub	FRAC % Barren soil
PD	38.7%	12.4%	15.1%	5.8%	4.9%	23.1%
105K2	21.8%	12.7%	25.1%	12.2%	4.7%	23.4%
FW105C2	9.7%	18.6%	30.9%	11.8%	3.1%	25.8%
105K2-PD	-16.9%	0.3%	10.0%	6.4%	-0.2%	0.3%
FW105C2-PD	-29.0%	6.2%	15.8%	6.0%	-1.8%	2.7%

Central Africa

In Table 12 the simulated Central African climate anomalies for annual mean Surface Air Temperature (SAT), Precipitation (P), Evaporation (E) and the E minus P anomalies (E-P) are shown for PD, 105K2 and FW105C2, as well as the simulated 105K2 minus PD and FW105C2 minus PD differences. Similar to the previous regions, the largest reduction in annual mean SAT in Central Africa occurs in the FW105C2 experiment (3.5 °C lower than PD), as compared to the 105K2 experiment (2.8 °C cooler than PD). Similar to East Africa, the magnitude of the SAT anomalies in Central Africa is much smaller compared to the SAT anomalies of North and West Africa. Lower annual mean P and E anomalies accompanied these SAT reductions, with the largest reductions occurring in the FW105C2 simulation (178.2 mm/a or 15.7% less P and 107.8 mm/a or 10.8% less E relative to PD), as compared to the 105K2 experiment (133.8 mm/a or 11.8% less P and 64.7 mm/a or 6.5% less E relative to PD). Overall the net impact of these E and P anomalies resulted in E minus P anomalies that suggest an overall drying in Central Africa relative to PD in both the 105 kya-like climate state and the HE 9-like climate state. In both the FW105C2 and 105K2 experiments, the E minus P anomalies were similar, and thus the drying in each experiment was of equal magnitude.

Table 12: Simulated Central African Climate Anomalies for the annual mean Surface Air Temperature (SAT), Precipitation (P), Evaporation (E) and E minus P anomalies (E-P) simulated for the 105K2 and FW105C2 simulations relative to present-day (PD)

Name of Model Output	Sat (°C)	P (mm/a)	E (mm/a)	E-P (mm/a)
PD	19.8	1131.4	997.6	-133.8
105k2	17.0	997.6	932.9	-64.7
FW105C2	16.3	953.2	889.8	-63.4
105K2-PD	-2.8	-133.8	-64.7	69.1
FW105C2-PD	-3.5	-178.2	-107.8	70.4

As illustrated in Table 13, there were reductions in the areal coverage of broadleaf trees, and increases in the areal coverage of needleleaf trees, C3 grasses, C4 grasses, shrubs and barren soil in both the FW105C2 and the 105K2 simulations. The model simulations show that the largest reductions in broadleaf tree coverage occurred in the FW105C2 experiment (56.7% less than PD, as compared to the 105K2 simulation (50.2 % less than PD). The increases in the areal coverage of C3 grasses, C4 grasses, shrub trees and barren soil, relative to PD, varied very little from each other between the 105K2 and FW105C2 simulations (See Table 13). However, there were significant differences in the magnitude of change between the two simulations for needleleaf tree coverage relative to PD. The model simulations show that the greatest increase in needleleaf trees occurred in the FW105C2 simulations (31.4 % more than PD, as compared to the 105K2 simulation (20.0 % more than PD). It is important to note that there was very little expansion of barren soil in both the 105K2 and FW105C2 experiments (less than 0.4%).

Table 13: Simulated Fractional Vegetative Coverage Anomalies (FRAC %) for the Five Plant Functional Types and Barren soil in Central Africa for the 105K2 and FW105C2 experiments relative to present-day

Name of Model Output	FRAC % Broadleaf	FRAC % Needleleaf	FRAC % C3	FRAC % C4	FRAC % Shrub	FRAC % Barren soil
PD	67.5%	12.8%	7.9%	2.8%	8.9%	0.1%
105K2	17.3%	32.8%	27.4%	10.9%	11.1%	0.5%
FW105C2	10.8%	44.2%	24.9%	10.2%	9.6%	0.4%
105K2-PD	-50.2%	20.0%	19.5%	8.1%	2.2%	0.4%
FW105C2-PD	-56.7%	31.4%	17.0%	7.4%	0.7%	0.3%

South Africa

In Table 14, the simulated South African climate anomalies for the annual mean Surface Air Temperature (SAT), Precipitation (P), Evaporation (E) and the E minus P anomalies (E-P) are shown for PD, 105K2 and FW105C2, as well as the simulated 105K2 minus PD and FW105C2 minus PD differences. Similar to the results for the other regions, the largest reduction in annual mean SAT in South Africa occurred in the FW105C2 simulation (3.0°C lower than PD), as compared to the 105K2 simulations (2.5 °C cooler than PD). However, model simulations show that South Africa experienced the smallest reduction in SAT, relative to PD, among all the regions. Unlike Central and West Africa, higher annual mean P and E anomalies accompanied these SAT reductions in South Africa in both climate states. The largest increases occurred in FW105C2 simulation (55.4 mm/a or 7.6% more P and 67.9 mm/a or 11% more E, relative to PD), as compared to the 105K2 simulation (50.6 mm/a or 6.9% more P and 75.7 mm/a or 12.2% more E, relative to PD). The overall net impact of these E and P anomalies resulted in E minus P anomalies that suggest an overall drying in South Africa relative to PD in both the 105 kya-like climate state and the HE 9-like climate state, although drying was less extensive in the HE 9-like climate state, relative to PD. It should also be noted that drying was less extensive in both climate states, as compared to the drying experienced in the other African regions.

Table 14: Simulated South African Climate Anomalies for the annual mean Surface Air Temperature (SAT), Precipitation (P), Evaporation (E) and E minus P anomalies (E-P) simulated for the 105K2 and FW105C2 simulations relative to present-day (PD)

Name of Model Output	Sat (°C)	P (mm/a)	E (mm/a)	E-P (mm/a)
PD	16.2	730.8	620.0	-110.8
105K2	13.7	781.4	695.7	-85.7
FW105C2	13.2	786.2	687.9	-98.3
105K2-PD	-2.5	50.6	75.7	25.1
FW105C2-PD	-3.0	55.4	67.9	12.5

As illustrated by Table 15, the model simulations revealed that in both the 105 kya-like climate state and the HE 9-like climate state there were small increases in the areal coverage of broadleaf trees (4.4% more in 105K2 and 3.3 % more in FW105C2), C4 grasses (8.5% more in 105K2 and 5.0% more in FW105C2) and barren soil (0.7% more in 105K2 and 0.6% more in FW105C2) and small reductions in shrubs (1.2% less in 105K2 and 1.0% less in FW105C2), relative to today. The most significant changes were the large reductions in needleleaf trees and the large increases in C3 grasses. The model simulations show that needleleaf tree coverage was reduced by 27.7 % in the 105K2 simulations, as compared to the 23.9 % reduction in the FW105C2 simulation. There was also 15.4 % more C3 grass coverage than PD in the 105K2 simulations, as compared to the 16.1 % expansion of C3 grasses, relative to PD, in the FW105C2 simulation. Similar to Central Africa, the South African simulation showed that there was very little expansion of barren soil in both the 105K2 and FW105C2 simulations (less than 0.7% in both simulations).

Table 15: Simulated Fractional Vegetative Coverage Anomalies (FRAC %) for the Five Plant Functional Types and Barren soil in South Africa for the 105K2 and FW105C2 simulations relative to present-day

Name of Model Output	FRAC % Broadleaf	FRAC % Needleleaf	FRAC % C3	FRAC % C4	FRAC % Shrub	FRAC % Barren soil
PD	17.9%	34.8%	36.6%	8.8%	1.5%	0.3%
105k2	22.3%	7.1%	52.0%	17.3%	0.3%	1.0%
FW105C2	21.2%	10.9%	52.7%	13.8%	0.5%	0.9%
105K2-PD	4.4%	-27.7%	15.4%	8.5%	-1.2%	0.7%
FW105C2-PD	3.3%	-23.9%	16.1%	5.0%	-1.0%	0.6%

8.0 Discussion

In this section I discuss the results of each experiment in combination, and discuss whether the model reconstructions generally support the interpretations of late Pleistocene paleoenvironmental records discussed in Section 4.2. To clarify and expand on the results of this study, I will refer to colour figures of the climate model results. I will then interpret the relevance of these results to the "Out-of-Africa 2" theory.

Overall the model reconstructions show that the complex interaction between orbitally-controlled solar radiation and atmospheric CO_2 forcing at 105 kya produced a significant part of the cooling and drying in Africa at this time interval; however, the model also indicates that the climate perturbations caused by the freshwater forcing could have amplified the cooling and drying that was already taking place in Africa due to orbital and atmospheric CO_2 forcing. The results also suggest that vegetation feedbacks and subsequent albedo changes through the expansion of more open and dry landscapes may have also enhanced the cooling observed in both the 105K2 and FW105C2 climate model simulations. As illustrated in Figure 7.1 and 7.2, the model reconstructions showed coherent spatial SAT and SST cooling in the subtropical and tropical Atlantic Ocean in both the 105 kya-like climate state and the HE 9-like climate state, although the greatest reductions were simulated in the HE 9-like climate state. In Figure 7.1 (FW105C2 minus PD), we see that the SAT cooling produced in the HE 9-like climate state is centered in the North Atlantic but extends into the African continent. In the HE 9-like climate state the SAT cooling anomaly follows a trend where the magnitude of cooling decreases progressively from the northwestern tip of Africa down into Southern Africa. As noted earlier, the largest cooling in the FW105C2 minus PD simulation occurred in North and West Africa (4.9 °C cooling in North Africa and 4.3 °C cooling in West Africa relative to PD), followed by East Africa with a 3.9 °C cooling relative to PD, then Central Africa with a 3.5 °C cooling relative to PD and then South Africa with a 3.0 °C cooling relative to PD. In the model heat transport is parameterized by Fickian diffusion (based on Fick's law which describes macroscopic transport of molecules by a concentration gradient). Model simulations suggest that as the North Atlantic Ocean chilled, large quantities of warm tropical air were transported polewards due to the larger inter-hemispheric surface pressure gradient, caused by the freshwater perturbation and its associated high-latitude cooling. The climatic repercussion in Africa was a cooling of the overlying atmosphere, as its heat

was lost to the growing cold SAT anomaly in the North Atlantic.

These abnormally cold SAT and SST anomalies observed in the FW105C2 simulation may be due to three different physical mechanisms. Firstly, the combined effect of the reduced atmospheric CO_2 and the orbital configuration at 105 kya. The determination and quantification of the relative contribution of the reduced atmospheric CO_2 effect and the effect of the orbital insolation configuration at 105 kya on the simulated climate at this time interval are beyond the scope of this study. However, it should be noted that it is known that the reduced atmospheric CO_2 partial pressure leads to a reduction of radiative forcing and thus to a global cooling (Hughes and Weaver, 1994). Secondly, this cooling effect in the African continent may have also been amplified by vegetation feedbacks and subsequent albedo changes through the expansion of dryland vegetation and the loss of rainforest. Thirdly, the enhanced cooling of the African continent and in the Atlantic Ocean may have been amplified by the influx of freshwater into the North Atlantic. The amplification of these cold SST and SAT anomalies in subtropical and tropical Atlantic in the FW105C2 simulation aligns favorably with the MOC and SSS anomalies produced in the FW105C2 simulation, which were also significantly reduced. The decrease in MOC in the FW105C2 simulation is caused by the development of a low-salinity cap over the North Atlantic that prevents sinking and formation of NADW, which in turn is due to the reduction in surface water density in the North Atlantic due to the injection of freshwater. As a result of the reduced formation of NADW, less warm water flowed northward in the model causing widespread cooling in the North Atlantic region to occur. These results are generally consistent with those of other modeling studies that show a slowdown of NADW and reduced MOC in the North Atlantic in response to a North Atlantic freshwater input (Manabe and Stouffer, 1997; Schiller et al., 1997). The reductions in SSTs are also consistent with McIntyre et al. (1976) interpretations that HE were associated with a cooling of the sub-polar Atlantic Ocean on the order of 4°C.

In Figure 7.2, the annual mean SAT anomalies are illustrated for 105K2 minus PD. This figure shows that the largest cooling in SAT in Africa, relative to PD, emanates from its center. As noted earlier, the largest cooling occurred in East and Central Africa (2.7 °C cooling in East Africa and 2.8 °C cooling in West Africa, relative to PD), followed by North Africa (2.6°C cooling relative to PD), and then West and South Africa, which both experienced 2.5°C cooling relative to PD. Unlike the results of the FW105C2 simulation, there is less regional variation in the SAT

anomalies. The cold SAT and SST anomalies observed in the 105K2 simulation can be ascribed solely to the combined effect of the reduced CO_2, the orbital configuration at 105 kya and vegetation feedbacks and subsequent albedo changes through the expansion of dryland vegetation and the loss of rainforest.

The amplified cooling effect of the freshwater forcing on the 105 kya-like climate state is further illustrated in Figure 7.3, which illustrates the annual mean SAT anomaly between the 105K2 and the FW105C2 experiment (105K2 minus FW105C2). This figure shows that the air mass overlying the Atlantic Ocean and the African continent was much warmer in the 105 kya-like climate state (spreading center in red in Figure 7.3) relative to the HE 9-like climate state. Although the pattern and magnitude of the SAT and SST anomalies vary between the two climate states, both the 105K2 and the FW105C2 simulations produced a regionally synchronous cold SAT anomaly throughout the African continent and throughout the subtropical and tropical Atlantic. These SAT anomalies relative to PD can be further examined by comparing Figure 7.2 and 7.3 to Figure 7.4 (simulated annual mean SAT for PD). The model's ability to simulate an amplified cooling in annual mean SAT in Africa in the FW105C2 simulation supports the previous interpretation of deMenocal (1995, 2004) inferring that cold SST anomalies in the North Atlantic and a reduction in the MOC can be linked with African aridity in the late Pleistocene.

(7.1)

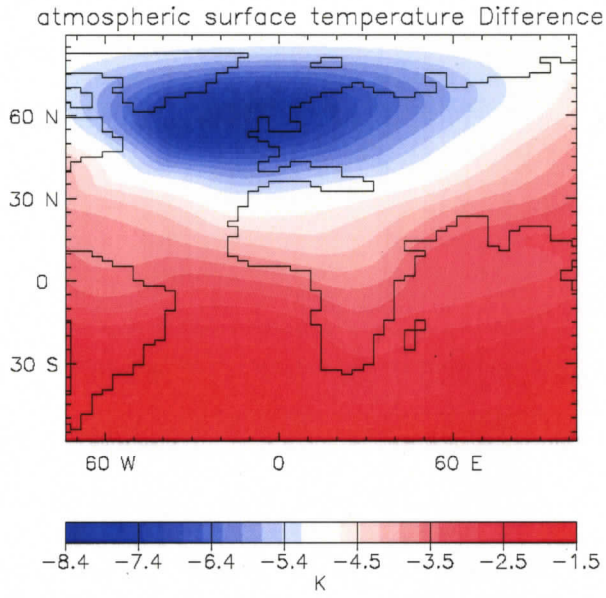

(7.2)

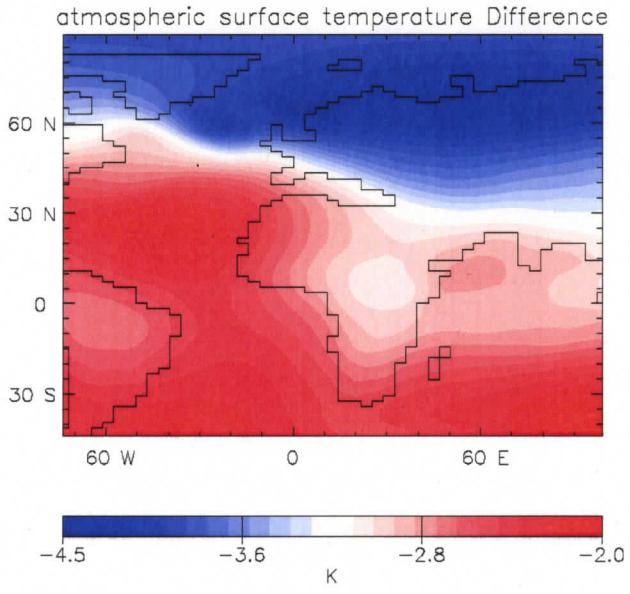

Figure 7.1 –7.2: Simulated annual mean Surface Air Temperature (SAT) anomaly relative to present (PD): **7.1** Difference in SAT (K) between the FW105C2 simulation (under 105 kya BP orbital, 230 ppmv CO_2 and 0.1 Sv freshwater forcing) and PD, **7.2** Difference in SAT (K) between the 105K2 simulation (under 105 kya BP orbital and 230 ppmv CO_2) and PD.

(7.3)

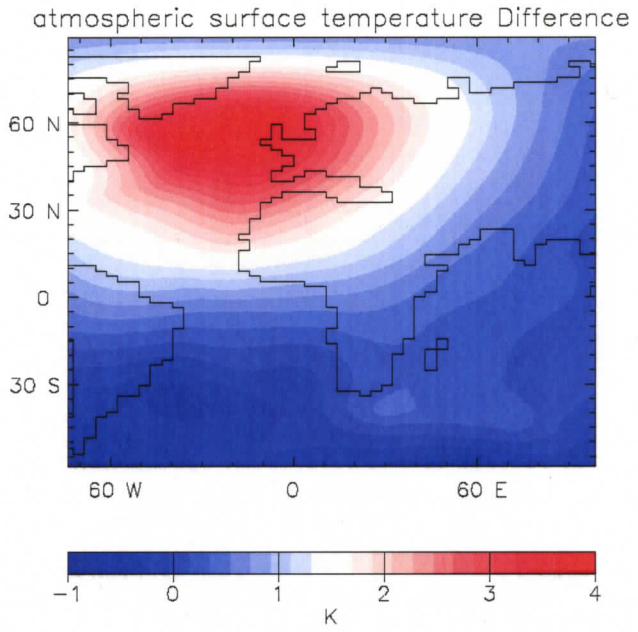

(7.4)

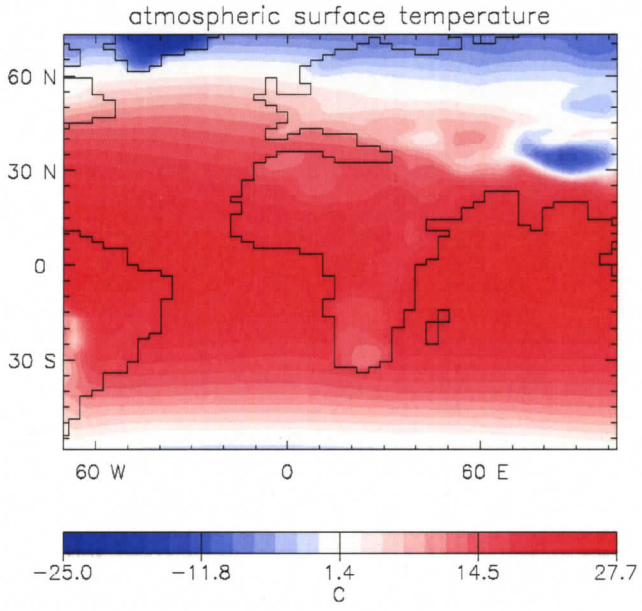

Figure 7.3 –7.4: Simulated annual mean Surface Air Temperature (SAT): **7.3** Difference in SAT (K) between the 105K2 simulation and the FW105C2 simulation, **7.4** Simulated Present-day SAT (°C)

The annual mean P and E anomalies generated by the model were also not as different as might be expected, as the model indicated a broad pattern of drying in all regions, except North Africa. In Figures 8.1 and 8.2 the results of the E minus P anomalies are illustrated for FW105C2 minus PD and 105K2 minus PD, respectively. As illustrated in these figures, the E minus P anomalies show that overall West, Central and East Africa experienced the most extensive drying, relative to today, in both the 105 kya-like and the HE 9-like climate states, although the largest reductions occurred in the FW105C2 simulation (area indicated in light red in Figure 8.1 and 8.2).

In contrast, the E minus P anomalies illustrated in these figures show that overall North Africa was wetter than today in both climate states, although it was significantly less wet in the HE 9-like climate state. However, as stated in the results section of this study, this outcome is due to the fact that the model presently overestimates rainfall over North Africa due to the fact that the areal coverage of the ITCZ band, parameterized in the model, is less narrow in the model than it is in nature. As a result the ITCZ and its rain belt, spreads further into North Africa than it should. Furthermore, the E minus P results also showed that although South Africa was overall drier than today in both climate states, the drying was less intense in the HE 9-like climate state and that overall the drying of South Africa relative to PD was less extensive than the drying seen in the other regions. This outcome may be attributable to the simulated southward shift of the ITCZ and its associated rain belt in the HE 9-like climate state due to the colder SST anomalies in the Atlantic. The amplification of regional drying in Africa between the two climate states is further illustrated in Figure 8.3, which illustrates that there was less extensive drying in the Sahel region of Africa in the 105 kya-like state (indicated in dark blue in Figure 8.3), relative to the HE 9-like climate state. Although North Africa was wetter than today in both the 105K2 and FW105C2 simulations, the fact that it was less moist in the HE 9-like climate state, relative to the 105 kya-like climate state (see Figure 8.3), indicates that the freshwater forcing caused a suppression of the moisture that otherwise would have been brought into the region due to orbital and atmospheric CO_2 forcing.

The E minus P anomalies associated with both climate states may be attributable to either the dual or separate effect of the simulated change in annual mean SATs in Africa or the simulated changes in the Atlantic SSTs. In the case of the annual mean SATs, the widespread cooling of SAT would have reduced evaporation over the African continent, which in turn would have reduced

precipitation over land. Moreover, the simulated drying of the African continent could also be ascribed to the reduced SSTs in the Atlantic also simulated by the model. Paleoclimate studies suggest that cold SST anomalies in the Atlantic greatly reduce evaporative moisture fluxes over the tropical Atlantic which feed the African monsoon rains (from the west) that drive moisture into the continent during boreal summer (Hastenrath, 1985). This theory is supported by the results presented in Table 4 and 5 and illustrated in these Figures 7.1 and 7.2, which show that SSTs were lower in the subtropical and tropical Atlantic than today, especially in the FW105C2 simulation.

The model's ability to simulate cold SST anomalies in the tropical Atlantic, as well as E minus P anomalies that suggest regional drying throughout Africa in the FW105C2 simulation, lends support to deMenocal's (1995) observations that modern occurrences of African Sahelian drought have been related to cold SSTs in the North Atlantic. These results are also consistent with paleoclimate studies that state that subtropical West, Central and East Africa were more arid when North Atlantic SSTs were cold during the late Pliocene and Pleistocene (deMenocal, 1995). Moreover, the E minus P anomalies associated with the freshwater forcing show that drying in Africa was most extensive along the Sahel region of Africa (see Figures 8.1, 8.2 and 8.3). The mechanism for this pattern of drying may be explained by the positioning of the ITCZ. These results agree favorably with the interpretations of Vidal and Arz (2004) that suggest that extreme cooling of the North Atlantic increases the interhemispheric SST gradient and as a result the ITCZ, and its associated rainfall belt, shift southwards. The southward migration of the ITCZ in the HE 9-like climate state may also provide a physical mechanism that explains why North Africa was less moist in the HE 9-like climate state, as compared to the 105 kya-like climate state.

(8.1)

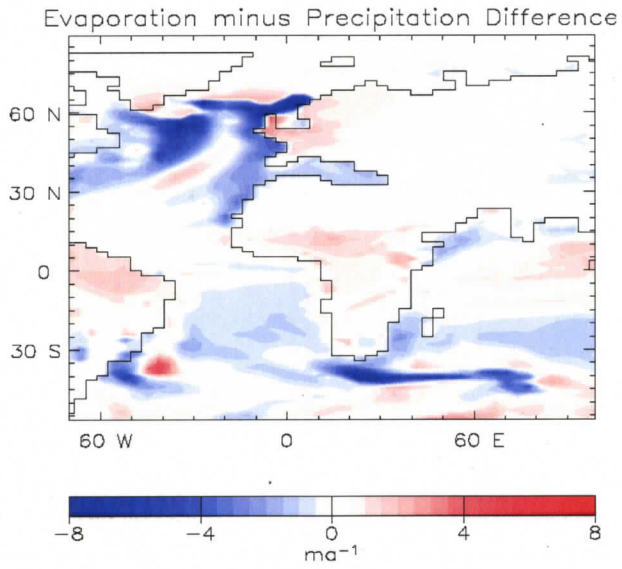

(8.2)

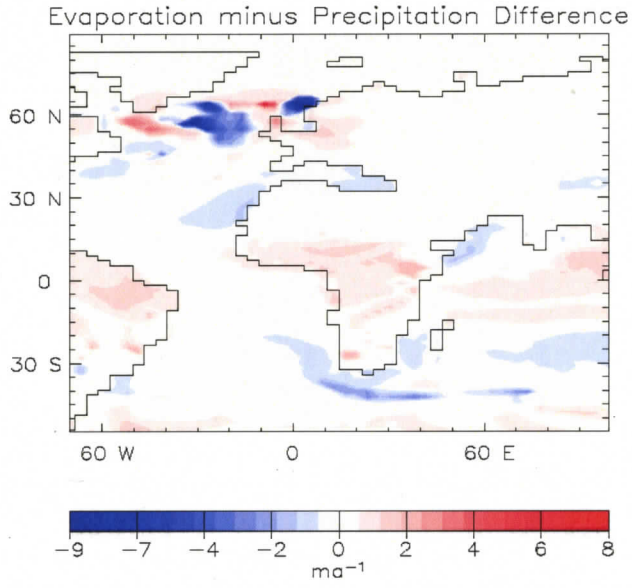

Figure 8.1 –8.2: Simulated mean annual E minus P anomaly relative to present (PD): **8.1** Difference in E minus P in meters per year (m/a) between the FW105C2 simulation (under 105 kya BP orbital, 230 ppmv CO_2 and 0.1 Sv freshwater forcing) and PD, **8.2** Difference in E minus P (m/a) between the 105K2 simulation (under 105 kya BP orbital and 230 ppmv CO_2) and PD.

(8.3)

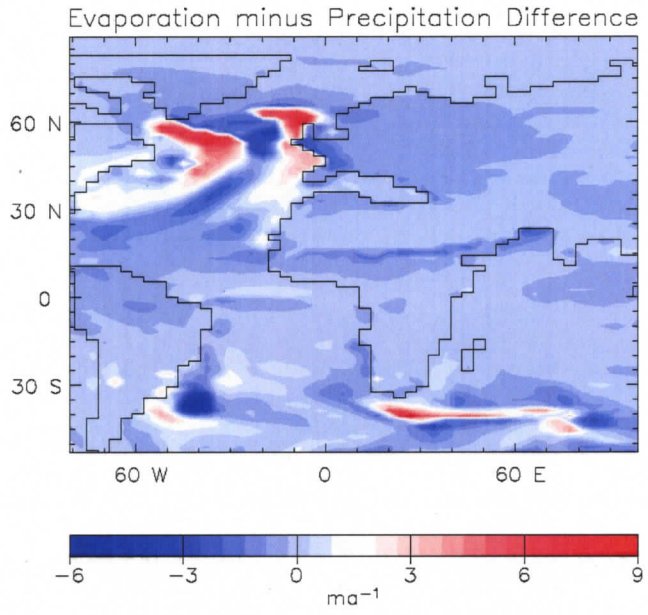

(8.4)

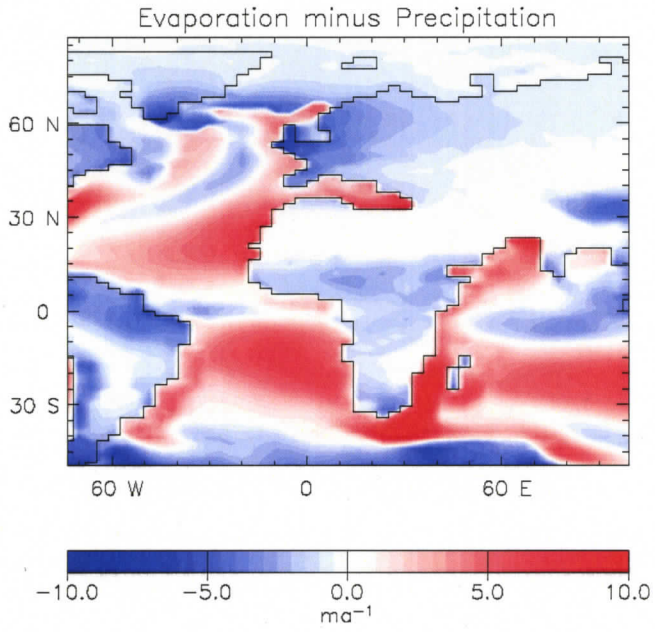

Figure 8.3 –8.4: Simulated annual mean E minus P anomaly: **8.3** Difference in E minus P (m/a) between the 105K2 simulation and the FW105C2 simulation, **8.4** Simulated present-day E minus P (m/a).

In Figure 9.1 –9.3, the regional areal coverage anomalies for broadleaf trees in Africa are presented for FW105C2 minus PD, 105K2 minus PD and 105K2 minus FW105C2. As illustrated in Figure 9.1 (FW105C2 minus PD) and 9.2 (105K2 minus PD), there was less broadleaf tree coverage relative to PD in West, Central and East Africa (area indicated in blue in Figure 9.1 and 9.2), and slightly more coverage in South Africa than today (area indicated in red in Figure 9.1 and 9.2). Model simulations show that there was no change in broadleaf tree coverage in North Africa relative to PD (PD simulation included no broadleaf trees in North Africa). The reduction of broadleaf tree coverage in these regions was more extensive in the FW105C2 simulation. The difference between the results of the two climate states can be seen in Figure 9.3 (105K2 minus FW105C2), which shows the areas where there was more broadleaf cover in the 105K2 simulation (area indicated in red in Figure 9.3), and the areas where there was more coverage in the FW105C2 simulation (area indicated in blue in Figure 9.3). The changes in broadleaf coverage in both climate states can be compared to Figure 9.4 (PD broadleaf tree coverage).

In Africa the majority of moist broadleaf forests are found in rainforests of equatorial Africa, and thus are characterized by warm, humid climates with year-round rainfall (Dupont et al., 2000). The large-scale reduction of broadleaf trees in Central, West and East Africa in both climate states suggests that these regions were drier than today, especially in the HE 9-like climate state. These results agree favorably with the E minus P anomalies and the SAT anomalies of this study which also show that West, Central and East Africa were drier and colder than today, especially in the HE 9-like climate state. In addition, the slight expansion of broadleaf trees in South Africa agrees to some extent with the E minus P anomalies and the SAT anomalies for South Africa which indicate that drying and cooling was minimal in South Africa, and thus it is expected that the broadleaf coverage would also be minimally reduced.

In the case of the 105K2 simulation, although it is difficult to attribute the broadleaf tree coverage trends to the reduction in atmospheric CO_2 or to the effect of the orbital configuration at 105 kya, the reduction of broadleaf trees in these regions, relative to PD, agrees favorably with what one would expect due to the development of colder and drier conditions in Africa. Furthermore, it can be surmised that the broadleaf coverage was further reduced in the HE 9-like climate state due to freshwater forcing that intensified the cold SAT anomalies in Africa. These results compare favorably with Dupont et al (2000) interpretation of marine and terrestrial

palynological data, which indicate that the extent of rain forest in West Africa was reduced during marine isotope sub-stage 5d (115 - 105 kya).

(9.1)

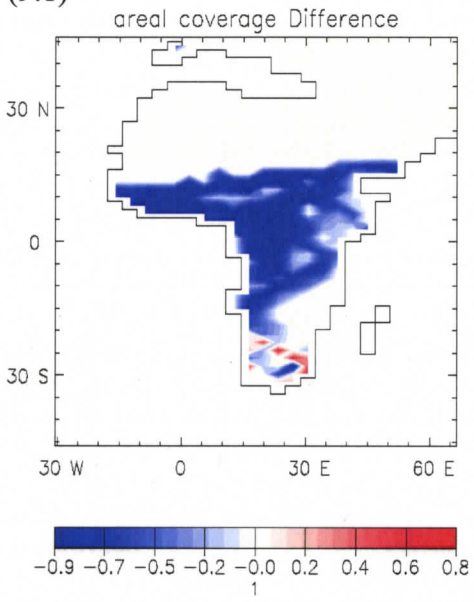

(9.2)

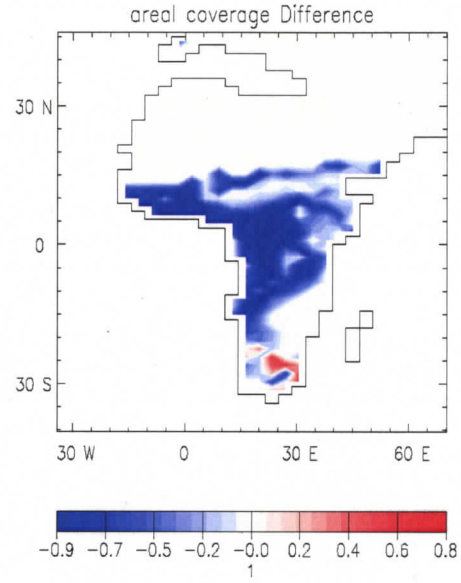

Figure 9.1 –9.2: Simulated fractional Broadleaf Tree Coverage (BTC) anomaly relative to present-day (PD): **9.1** Difference in BTC between the FW105C2 simulation (under 105 kya BP orbital, 230 ppmv CO_2 and 0.1 Sv freshwater forcing) and PD, **9.2** Difference in BTC between the 105K2 simulation (under 105 kya BP orbital and 230 ppmv CO_2) and PD.

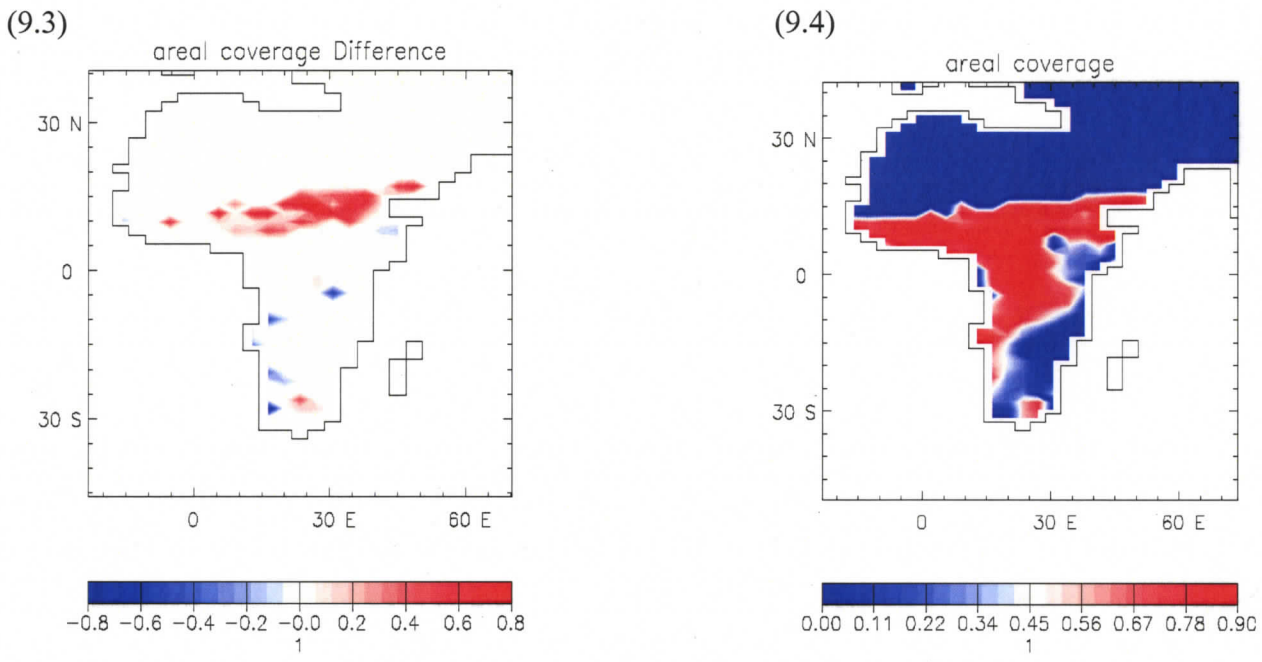

Figure 9.3 –9.4: Simulated fractional Broadleaf Tree Coverage (BTC): **9.3** Difference in BTC between the 105K2 simulation and the FW105C2 simulation, **9.4** Simulated present-day BTC.

In Figure 10.1 –10.3, the regional areal coverage anomalies for needleleaf trees in Africa are presented for FW105C2 minus PD, 105K2 minus PD and 105K2 minus FW105C2. As illustrated in Figure 10.1 (FW105C2 minus PD) and 10.2 (105K2 minus PD), the model simulations revealed that there were expansions of needleleaf trees in West, East and Central Africa (areas indicated in red in Figures 10.1 and 10.2) and contractions of needleleaf trees in South Africa, relative to today (areas indicated in blue in Figures 10.1 and 10.2). In North Africa there was no change from today (PD simulation included no needleleaf trees in North Africa). The expansion of needleleaf tree coverage in these regions was more extensive in the FW105C2 experiment (Figure 10.1). The difference between the results of the two climate states is clearly illustrated in Figure 10.3 (105K2 minus FW105C2), which indicates the areas where the needleleaf tree coverage was greater in the 105K2 experiment (area indicated in red in Figure 10.3) and the areas where there was more needleleaf tree coverage in the FW105C2 experiment (area indicated

in blue in Figure 10.3). The changes in needleleaf coverage in both climate states can be compared to Figure 10.4 (PD needleleaf vegetation).

The dense forest of evergreen needleleaf trees flourishes well in colder and drier climates (Woodward et al., 2004). By implication, these results suggest that in addition to being drier, West, Central and East Africa were also colder relative to today, especially in the HE 9-like climate state in which expansions were larger. These results also agree favorably with the E minus P anomalies and the SAT anomalies of this study which also show that West, Central and East Africa were drier and colder than today, especially in the HE 9-like climate state. Furthermore, the reduction of needleleaf trees seen in South Africa is somewhat consistent with the E minus P and SAT anomalies for South Africa as they indicate that South Africa experienced less drying and cooling, relative to PD, and therefore conditions would have been less conducive to needleleaf growth.

As in the case of the broadleaf tree coverage anomalies, it is the conclusion of this study that this shift in needleleaf tree coverage is also partly due to the combined cooling effect of reduced atmospheric CO_2 and the orbital configuration at 105 kya and the development of drier conditions in Africa. Furthermore, it is the conclusion of this study that the needleleaf coverage was enhanced in the HE 9-like climate state due to freshwater forcing that intensified the cooling and drying of West, Central and East Africa.

(10.1)

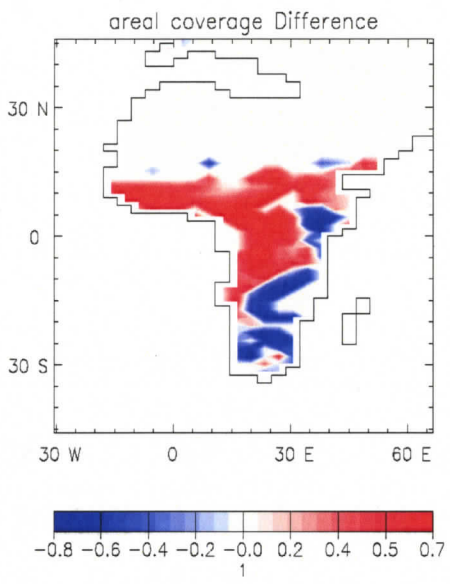

(10.2)

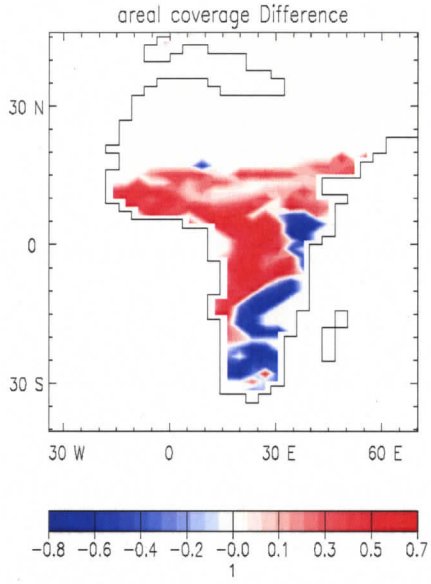

(10.3)

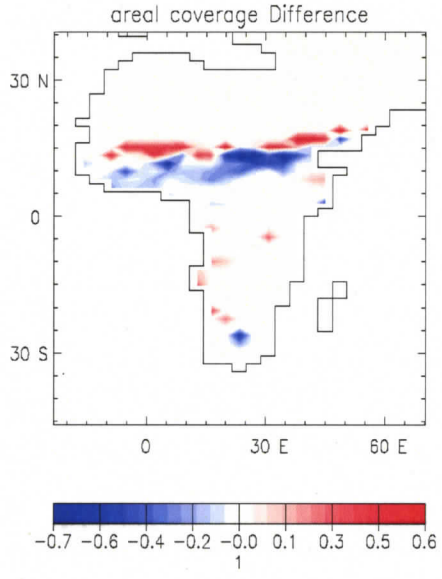

(10.4)

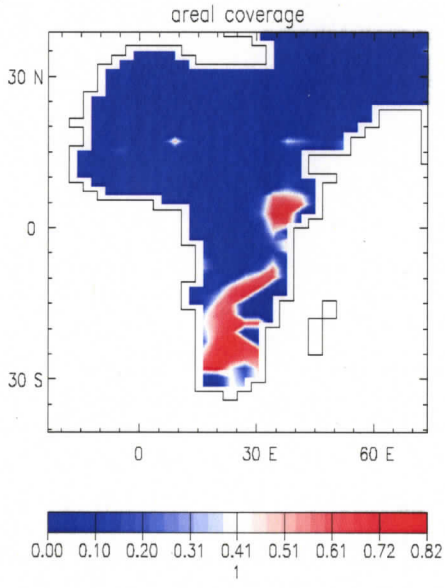

Figure 10.1 –10.4: Simulated fractional Needleleaf Tree Coverage (NTC) anomaly: **10.1** Difference in NTC between the FW105C2 simulation (under 105 kya BP orbital, 230 ppmv CO_2 and 0.1 Sv freshwater forcing) and PD, **10.2** Difference in NTC between the 105K2 simulation (under 105 kya BP orbital and 230 ppmv CO_2) and PD, **10.3** Difference in NTC between the 105K2 simulation and the FW105C2 simulation, **10.4** Simulated present-day NTC.

In Figure 11.1 –11.3, the regional areal coverage anomalies for C3 grasses in Africa are presented for 105K2 minus PD, FW105C2 minus PD and 105K2 minus FW105C2. As illustrated in Figure 11.1 (FW105C2 minus PD) and 11.2 (105K2 minus PD), there were increases in the areal coverage of C3 grass in East, Central and South Africa (areas indicated in red in Figures 11.1 and 11.2), and reductions in C3 grass coverage in North and West Africa (areas indicated in blue in Figures 11.1 and 11.2), relative to PD. However, the reduction of C3 grass coverage in North and West Africa was more extensive in the FW105C2 experiment, and the expansion in East and South Africa was also larger in FW105C2 experiment. The difference between the results of the two climate states is clearly illustrated in Figure 11.3 (105K2 minus FW105C2), which indicates the areas where the C3 grass coverage was greater in the 105 kya-like climate state (area indicated in red in Figure 11.3) and the areas where the C3 grass coverage was greater in the HE 9-like climate state (area indicated in blue in Figure 11.3).

In general C3 grasses are adapted to cool and wet environments, and are found in abundance around the margins of cool deserts (Woodward et al., 2004). If I were to use modeled vegetation results exclusively to infer climatic conditions I would expect North and West Africa to be somewhat less cool and wet than today, and East, Central and South Africa to be somewhat cooler and wetter than today. However, these results are not consistent with the model simulated E minus P anomalies and the SAT anomalies of this study which show that West, Central, East and South Africa were drier and colder than today, especially in the HE 9-like climate state. Furthermore, there are discrepancies between the vegetation results and the E minus P and SAT anomalies for North Africa, as the SAT anomalies suggest that North Africa was colder and the E minus P anomalies show that it was wetter than today. A possible mechanism for the C3 grass coverage anomalies may be that the plants are reacting to the lower atmospheric CO_2 concentrations or may be the result of competition between the C3 grasses and the other vegetation types that perform better under the simulated climate conditions. However, the determination of a relationship between the lower atmospheric CO_2 concentrations and the C3 grass distribution changes is beyond the scope of this study. As a result it is the conclusion of this study that the vegetation shifts are due to changes in climate and lower atmospheric CO_2 concentrations and intra-species competition prescribed by the model. Overall these results suggest that grasslands

expanded in East, Central and South Africa (more open landscape) and that grasslands were reduced in North and West Africa.

(11.1)

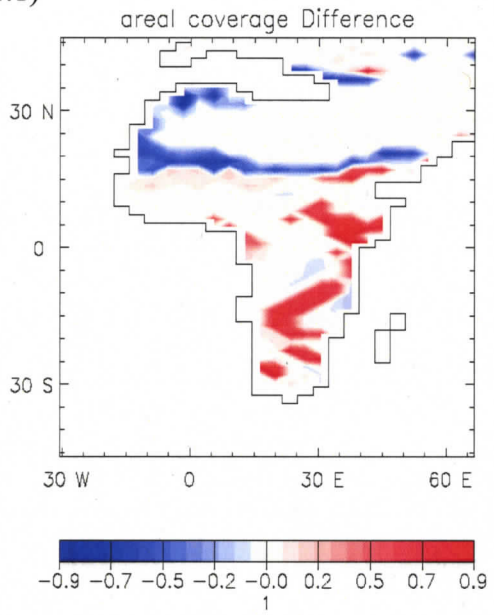

(11.2)

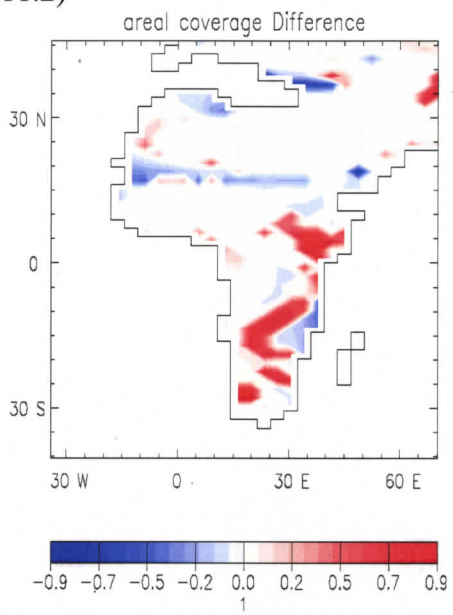

(11.3)

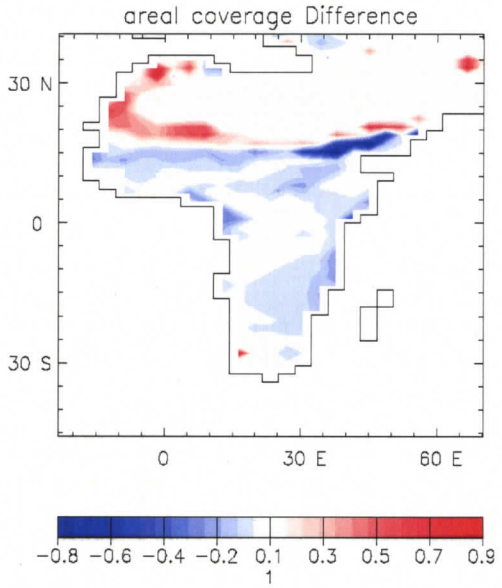

(11.4)

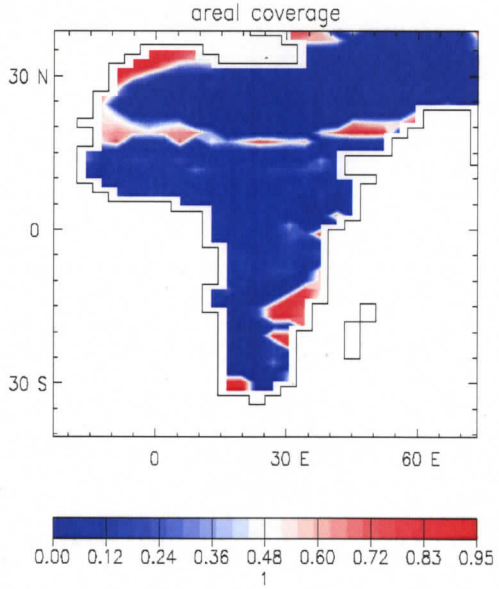

Figure 11.1 –11.2: Simulated fractional C3 grass Coverage (C3C): **11.1** Difference in C3C between the FW105C2 simulation (under 105 kya BP orbital, 230 ppmv CO_2 and 0.1 Sv freshwater forcing) and PD, **11.2** Difference in C3C between the 105K2 simulation (under 105 kya BP orbital and 230 ppmv CO_2) and PD **11.3** Difference in C3C between the 105K2 simulation and the FW105C2 simulation, **11.4** Simulated present-day C3C.

In Figure 12.1 –12.3, the regional areal coverage anomalies for C4 grasses in Africa are presented for 105K2 minus PD, FW105C2 minus PD and 105 minus FW105C2. As illustrated in Figure 12.1 (FW105C2 minus PD) and 12.2 (105K2 minus PD), there were reductions in the areal coverage of C4 grasses in North Africa relative to PD (areas indicated in blue in Figures 12.1 and 12.2), whereas the results show that there were the expansions of C4 grasses in East, West, Central and South Africa (areas indicated in red in Figures 12.1 and 12.2), relative to today, although the simulated changes were small in each region. The difference between the areal coverage of C4 grasses between the two experiments is clearly illustrated in Figure 12.3 (105K2 minus FW105C2), which shows the areas where the coverage of C4 grasses was greater in the 105K2 experiment (area indicated in red in Figure 12.3) and the regions where the C4 grasses was greater in the FW105C2 experiment (area indicated in blue in Figure 12.3). The changes in C4 grass coverage in both climate states can be compared to Figure 12.4 (PD C4 vegetation).

In general C4 grasses are generally confined to arid climates (hot and dry environments) (Woodward et al., 2004). As before, the modeled vegetation results would imply that North Africa was somewhat less arid, and East, West, Central and South Africa were more arid than today, in both climate states. The results of the C4 grass coverage anomalies agree favorably with the E minus P and the SAT anomalies found in the model simulation which show that North Africa was wetter and colder than today and that East, West, Central and South Africa were more arid than today, especially in the HE 9-like climate state. As in the case with the modeled C3 grass coverage anomalies, a possible mechanism for the C4 grass coverage anomalies may be that the plants are also reacting to the lower atmospheric CO_2 concentrations and simulated climate changes or may be the result of competition between the C4 grasses and the other vegetation types that are better adapted to arid climate conditions (needleleaf trees and barren soil). Overall the results suggest that there was an expansion of grasslands, albeit small, in West, East, Central and South Africa (more open landscape) and a contraction of grasslands in North Africa. However, later in this study it will be revealed that like the C3 grass coverage anomalies, the reduction in C4 grass coverage in North was compensated primarily by barren soil (suggestive of more open landscape).

(12.1)

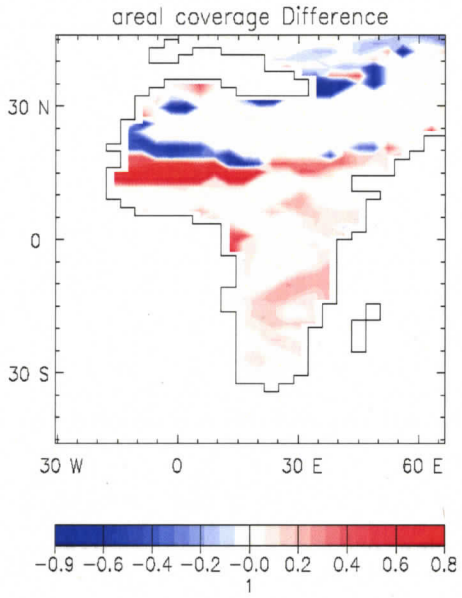

(12.2)

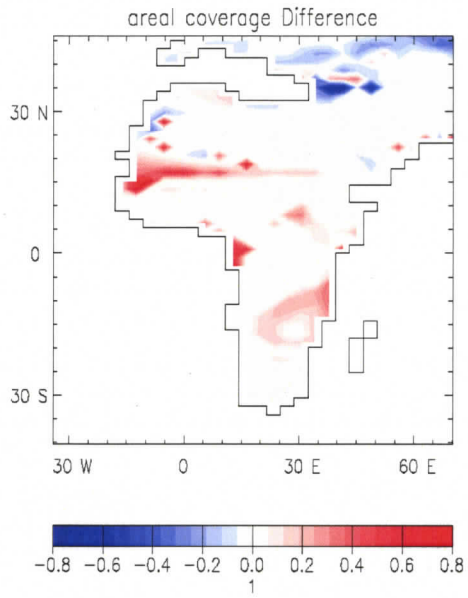

(12.3)

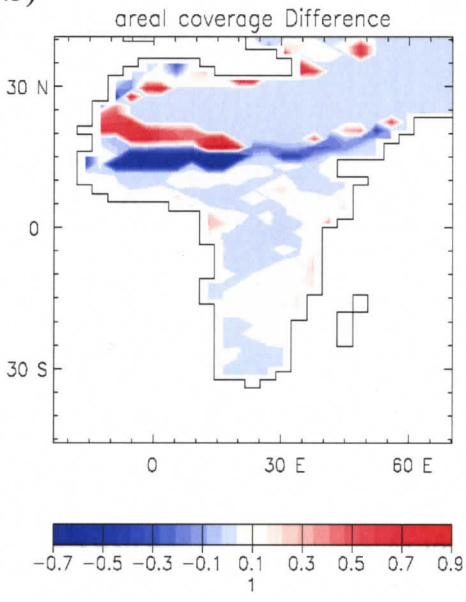

(12.4)

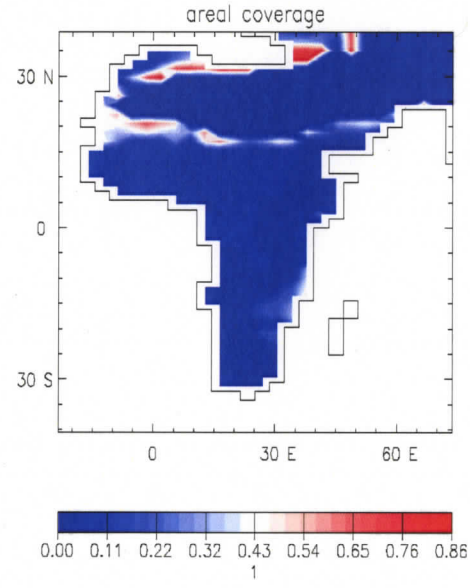

Figure 12.1 –12.4: Simulated fractional C4 grass Coverage (C4C): **12.1** Difference in C4C between the FW105C2 simulation (under 105 kya BP orbital, 230 ppmv CO_2 and 0.1 Sv freshwater forcing) and PD, **12.2** Difference in C4C between the 105K2 simulation (under 105 kya BP orbital and 230 ppmv CO_2) and PD, **12.3** Difference in C4C between the 105K2 simulation and the FW105C2 simulation, **12.4** Simulated present-day C4C.

In Figure 13.1 –13.3, the regional areal coverage anomalies for shrub trees in Africa are presented for 105K2 minus PD, FW105C2 minus PD and 105K2 minus FW105C2. As illustrated in Figure 13.1 (FW105C2 minus PD) and 13.2 (105K2 minus PD), the model simulations indicate that there was a small expansion of shrub trees in Central Africa (2.2 % more in 105K2 and 0.7 % more in FW105C2) (areas indicated in red in Figure 13.1 and 13.2), and small contractions in East (0.2% less in 105K2 and 1.8% less in FW105C2), West (0.1% less in 105K2 and 8.0% less in FW105C2) and South Africa (1.2% less in 105K2 and 1.0% less in FW105C2)(areas indicated in blue in Figure 13.1 and 13.2), relative to PD. There were no changes in the areal coverage of shrub vegetation in North Africa relative to today (PD simulation included no shrub trees in North Africa). Although the changes in the areal coverage of shrub tress were generally small from today, the contraction of shrub coverage in West and East Africa were more extensive in the FW105C2 experiment. The difference between the areal coverage of shrub trees between the two climate states is clearly illustrated in Figure 13.3 (105K2 minus FW105C2). The changes in shrub coverage in both climate states can also be compared to Figure 13.4 (PD shrub vegetation).

In general, most shrubs are adapted to arid conditions; therefore, the model simulated vegetation results suggest that East, West and South Africa became somewhat less arid than today, whereas Central Africa became somewhat more arid. At first glance, these modeled vegetation results appear to contradict with the SAT and E minus P anomalies of this study, which together show that the African continent became generally more arid in both climate states, especially in the HE 9-like climate state. Again, due to the limited scope of this study it is concluded that the vegetation shifts are due to changes in climate and lower atmospheric CO_2 concentrations, as well as intra-species competition between shrub trees and the other vegetation types that are better adapted to arid climate conditions (needleleaf trees and barren soil). Overall these results suggest that there was an expansion of shrub lands in Central Africa and small contractions of shrub lands in West, East, Central and South Africa.

(13.1)

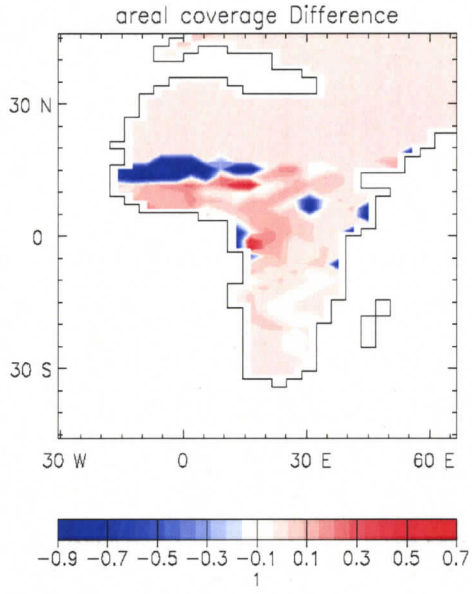

(13.2)

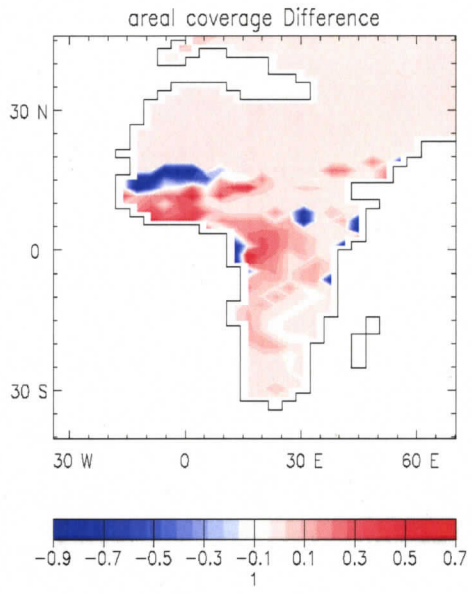

(13.3)

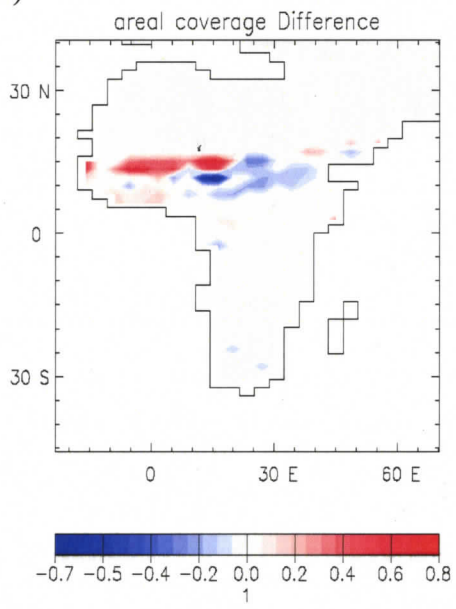

(13.4)

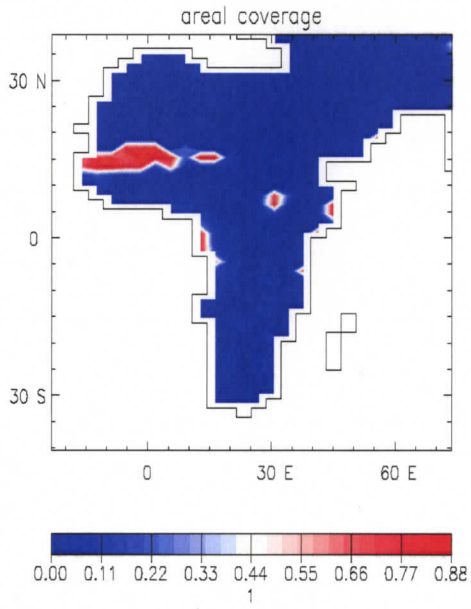

Figure 13.1 –13.4: Simulated fractional Shrub Vegetation Coverage (SVC): **13.1** Difference in SVC between the FW105C2 simulation (under 105 kya BP orbital, 230 ppmv CO_2 and 0.1 Sv freshwater forcing) and PD, **13.2** Difference in SVC between the 105K2 simulation (under 105 kya BP orbital and 230 ppmv CO_2 and PD, **13.3** Difference in SVC between the 105K2 simulation and the FW105C2 simulation, **13.4** Simulated present-day SVC.

In Figure 14.1 –14.3, the regional areal coverage anomalies for barren soil in Africa are presented for 105K2 minus PD, FW105C2 minus PD and 105K2 minus FW105C2. As illustrated in Figure 14.1 (FW105C2 minus PD) and 14.2 (105K2 minus PD), the areal coverage of barren soil increased in each region; however, the largest expansion of barren soil occurred in the FW105C2 experiment. Furthermore, the largest expansions of barren soil occurred in North and West Africa (area indicated in red in Figure 14.1), whereas the increases in the remaining regions were negligible. The difference between the areal coverage of barren soil between the two experiments is clearly illustrated in Figure 14.3 (105K2 minus FW105C2), which indicates the areas where the coverage of barren soil was greater in the FW105C2 experiment (area indicated in blue in Figure 14.3). These results compare favourably with the SAT and E minus P anomalies of this study which indicate that the African continent became more arid at this interval, especially in the HE 9-like climate state, conditions known to be conducive to the development of desert-like conditions.

(14.1)

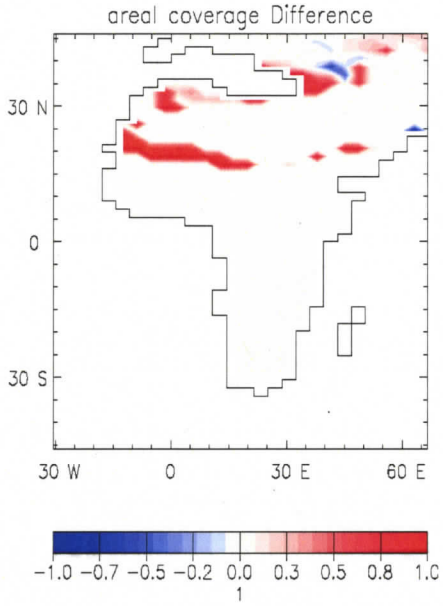

(14.2)

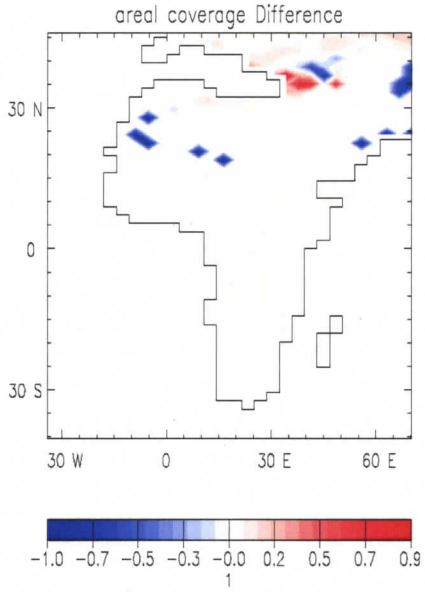

(14.3)

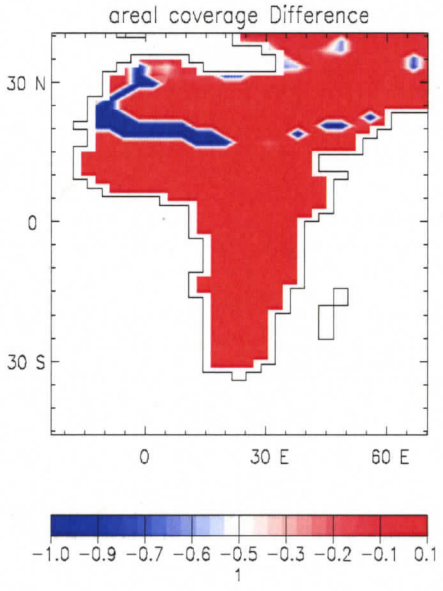

(14.3)

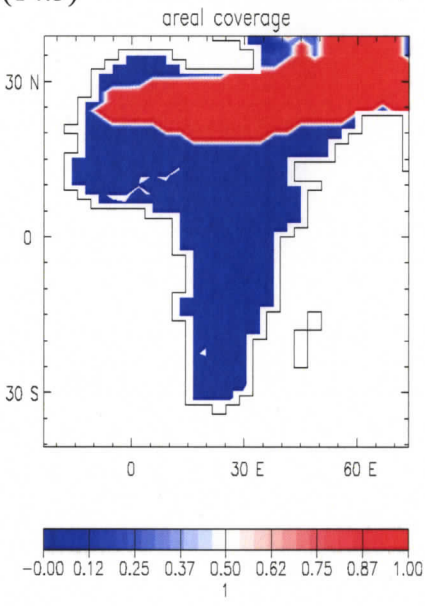

Figure 14.1 –14.4: Simulated fractional Barren Soil Coverage (BSC): **14.1** Difference in BSC between the FW105C2 simulation (under 105 kya BP orbital, 230 ppmv CO_2 and 0.1 Sv freshwater forcing) and PD, **14.2** Difference in BSC between the 105K2 simulation (under 105 kya BP orbital and 230 ppmv CO_2) and PD, **14.3** Difference in BSC between the 105K2 simulation and the FW105C2 simulation, **14.4** Simulated present-day BSC.

Another interesting feature of these model simulations is the fact that the greatest changes in vegetation between the 105K2 simulation and the FW105C2 simulation occurred in the Sahel region of Africa (see Figures 9.3, 10.3, 11.3, 12.3, 13.3 and 14.3). This pattern is similar to the pattern seen in the E minus P anomalies associated with the freshwater forcing. As previously stated the mechanism for the development of this pattern of vegetation change, relative to PD, may be explained by the position of the ITCZ, and its sensitivity to SSTs. These results also agree favorably with the interpretations of Vidal and Arz (2004) that extreme cooling of the North Atlantic is associated with a southward shift of the ITCZ and its associated rainfall belt. The southward shift of the ITCZ was observed and confirmed through the comparative analysis of the simulated annual mean precipitation plots of the 105K2 simulation and the FW105C2 simulation (not shown here). As a result it is the conclusion of this study that the pronounced vegetation changes (shifts towards more open landscapes and arid-adapted vegetation) simulated in the Sahel region in the FW105C2 simulation are due to the southward migration of the ITCZ.

Overall modelled mean annual E minus P and SAT anomalies show that the greatest cooling, relative to today, took place in North, Central, West and East Africa and the greatest drying took place in West, Central and East Africa, especially in the HE 9-like climate state. Conversely, less extensive drying and cooling took place in South Africa, relative to today, especially in the HE 9-like climate state. The simulated areal vegetation coverage anomalies also support this trend as the results suggest that overall arid conditions were most pronounced in North, West, Central and East Africa. In contrast the vegetation changes indicative of a cooling and drying relative to PD were less pronounced in South Africa.

These results compare favorably with Dupont and Hooghiemstra's (1989) interpretations that West African rainforest was strongly reduced during oxygen isotope substage 5d (115 -105 kya). These results are also consistent with Leuschner et al.'s (2004) and Reichart et al.'s (1998) interpretations of eolian dust concentrations found in the western and northern Arabian Sea that indicate that during the cold stadial of 5d (115 –105 kya) large quantities of dust were deposited in this area, indicative of more arid conditions. Furthermore, the extensive expansion of barren soil occurred in North Africa lends support to Dupont and Hooghiemstra's (1989) interpretations that the desert in North Africa was more extensive during the last glacial cycle and their interpretations

of the tendency of the Saharan-Sahelian boundary to migrate back and forth between ca. 21° – 19° N during MIS 5. However, the less extensive drying and cooling in South Africa and the minimal expansion in barren soil simulated by the model are not consistent with Stokes et al.'s (1997) interpretation of the record of desert-dune formation in the Kalahari desert, which indicates that south-western Africa became extremely arid between 90 -110 kya (marine isotope sub-stage 5d-5b).

It is important to note that tracers of deep water production support the hypothesis that similar changes in NADW formation are coincident with climate change during the Younger Dryas, a 1,300 year long cold event that began about 13 kya (Boyle and Keigwin, 1987; Bond et al., 1997), that was also induced by meltwater influxes into the North Atlantic. Furthermore, paleoclimate studies have shown that vegetation responds quickly to climate changes, whereas the regrowth and spread of forests into grassland regions would require much longer time periods (Schefub et al., 2005). Therefore, in theory it can be surmised that the African and Atlantic Ocean climate changes induced by HE 9 may have potentially persisted for thousands of years.

The results of this study, namely the concurrent drying and cooling of North,West, East and Central Africa align well with not only the picture constructed by the African late Pleistocene paleoclimate data, but also with the migration theories that propose that a change in inland climate may have encouraged AMH to seek refuge on the Southern and Eastern coasts of Africa (Walter et al., 2000 and Stringer, 2000). Based on the fossil record, it appears that around 130 kya, AMH were living predominantly in the interior of East Africa, a period of intense drought in Africa that coincided with an Ice Age in Europe. Walter et al (2000) have argued that AMH might have sought refuge from the aridity of the African interior in the more hospitable climates of the coast. From the abundance of paleoclimate data, archaeological data and the results of this climate model study, the implication is that if AMH had become well-adapted to exploiting coastal marine resources and living on the coasts after 120 kya (Stringer, 2000), the development of hyper-arid conditions around 105 kya, which may have persisted into the late Pleistocene, may have encouraged AMH to retreat from their traditional terrestrial habitats towards the coasts again, if they were not already living there, and eventually migrate out of the African continent. Overall, the model simulations show that grasslands, needleleafs and barren soil expanded at the expense of rainforest during this interval, especially in the HE 9-like climate state.

In addition, the model results for the HE 9-like climate state suggest that the cold SST anomalies in the Atlantic were accompanied by a southward shift in the ITCZ and its associated rain belt. As a result, when comparing the two climate states we see that not only did the desert (barren soil) expand in North Africa, but also there were significant changes in moisture and expansion of dryland landscapes in the Sahel region of Africa. In human terms the more open and arid landscape in the Sahel region may have acted as a major barrier to AMH dispersal at this time, restricting movement into North Africa because much of the landscape would have been unsuitable for expanding human populations. As the cold and aridity intensified desert barriers, it may have reduced marine barriers and exposed more of the continental shelf along the African coasts. As mentioned previously the global sea-levels reached a highstand during MIS 5e with sea levels between 2 and 12 m above present (van Andel & Tzedakis, 1996); however, this was followed by a variable but progressive drop in sea levels to LGM lowstand between -118 and 135 m (Clark & Mix, 2002). Depending on the extent of sea-level passage east from the Horn of Africa could have occurred along the extended coastal shelf at this time.

The simulated changes in the Indian Ocean were also analyzed in this study, although the numerical results are not shown here. Model simulations revealed that SSTs, SATs, P and E were all lower in both climate states relative to PD, although the reductions were significantly larger in the FW105C2 simulation. In the 105K2 simulation SAT in the Indian Ocean was reduced by 2.4 °C and SST was reduced by 2.0 °C relative to PD, as compared to the FW105C2 simulation where SAT was reduced by 2.9 °C and SST was reduced by 2.4 °C. Moreover, the E minus P anomalies revealed that although the Indian Ocean was relatively colder in the FW105C2 simulation, it was equally wetter in both climate states, relative to PD. Although the results suggest that the Indian Ocean was wetter in both climate states, the colder SSTs and SATs in the Indian Ocean would have reduced the overall evaporative moisture fluxes feeding the Indian monsoon winds that bring moisture into East Africa and Arabia during the NH summer, thus reducing the amount of precipitation brought into these regions at this time. These results support the theory that the climatic impacts of HE may not be constricted to the Atlantic, but rather may be translated globally through oceanic teleconnections.

9.0 Conclusion

Climate is considered as an integral element that has been critical in early human migrations, perhaps not directly, but through its effects on the spatial distribution and abundance of water, plants and animals. Overall, the climate model results of this study support the general climate scenario outlined by the paleoclimate data, which together provide compelling evidence that Africa experienced profound shifts in its climate around 100 kya, which led to increasing aridity and the desiccation of biogeographic resources. Although the fossil record is still too fragmentary to establish precise correlations with paleoclimate records, by placing the African behavioural record of early human migrations within the context of ancient climate change, a general relationship between Pleistocene climate change and early human migration can be seen. Ultimately, the results of this study show that although both orbital and atmospheric CO_2 forcing played deterministic roles in African aridity at this discrete climatic period, the freshwater forcing in the North Atlantic is viewed to be a superimposed but primary factor affecting African climate. The development of cold conditions in Africa may have also been amplified through vegetation feedbacks, and subsequent albedo changes through the expansion of dryland vegetation and the contraction of rainforest. Based on these climate model results, supported by paleoclimate data, it is apparent that the cooling and drying would have rendered Africa unsuitable for hominid occupation, especially in North, West and Central Africa. In human terms, the pronounced cooling and drying in these regions would have modulated not only the African landscape, but also the spatial distribution of human populations. Ultimately these changes would have acted as a barrier to human dispersal, confining the geographical range of AMH to the more hospitable environments of East and South Africa. As theorized by Potts (1996), it is this climatic variability that, through consequent habitat variability and perhaps dwindling food and water resources due to changes in temperature and rainfall, drove the dynamics of geographical range in AMH.

For years a number of studies have postulated that climate variability on millennial-timescales, caused by rapid surging of ice sheets and fresh water capping of the North Atlantic, is not limited to the North Atlantic; however, for the most part this paradigm has remained enigmatic. The results of this study present compelling evidence that North Atlantic climate changes can be effectively propagated throughout the globe in order to induce seemingly simultaneous climate change as suggested by deMenocal (1995). In particular, these results lend support to the assertion

that African cooling and drying is associated with, not only low-latitude climate controls, but also high-latitude glacial stress such as HE.

These results, and the implications that they carry regarding the role of climate in the adaptations and migrations of early humans, relate not only to our past but also to our future. Presently, scientists are scrambling to find new and more precise means of understanding how climate has changed on various time scales in the past in order to help them understand and prepare for how climate may change in the future. The search for knowledge has been largely shaped by the analysis of many geological, chemical, biological and physical proxies of past climate. However, in recent years great strides have been made toward better correlations and integrations of the African hominin fossil record and paleoclimate datasets. It is argued here that the continued evaluation of the temporal and spatial characteristics of early hominin migrations within the broader context of paleoenvironmental changes will provide scientists with a unique diagnostic tool for investigating past and future climatic fluctuations.

In particular, it is my sincere hope that this study will help garner awareness of the demonstrable need to better understand how developing nations, like Africa, will be environmentally impacted as the global climate continues to change into the 21st century and beyond. Undeniably, if preventative measures are not taken now to understand the sensitivity of the African climate to future climate change scenarios, this continent's lack of scientific and technological capabilities will undeniably render it incapable of responding to future climate change and the lives of millions of Africans may be pushed beyond their ability to cope and survive--much as they once were some 100 kya.

10.0 References

Adams, J.M., (1997). Global land environments since the last interglacial. Oak Ridge National Laboratory, TN, USA. http://www.esd.ornl.gov/ern/qen/nerc.html

Adams J.M. & Faure H. (1997) (ed.s), QEN members. Review and Atlas of Palaeovegetation: Preliminary land ecosystem maps of the world since the Last Glacial Maximum. Oak Ridge National Laboratory, TN, USA. http://www.esd.ornl.gov/ern/qen/adams1.html

Arz, H.W., JuergenW. P. and Wefer, G., 1998. Correlated millennial-scale changes in surface hydrography and terrigenous sediment yield inferred from last-glacial marine deposits off northeastern Brazil. Quaternary Research, 50: 157-166

Arz, J.A., Arenillas, I., Soria, A.R., Alegret, L., Grajales-Nishimura, J.M., Liesa, C.L., Meléndez, A., Molina, E., and Rosales, M.C., 2001. Micropaleontology and sedimentology across the Cretaceous/Tertiary boundary at La Ceiba (Mexico): Impact-generated sediment gravity flows: Journal of South American Earth Sciences (in press).

Barron, E.J. & D. Pollard, 2002. High-resolution climate simulations of Oxygen Isotope Stage 3 in Europe. Quaternary Research 58: 296-309.

Bar-Yosef, O. 1995. The Origins of Modern Humans. Archaeology of Society in the Holy Land. pp.110 -123.

Behrensmeyer, B. and Chapman, A.K., 2002. Faunal change, environmental variability and late Pliocene hominin evolution. Journal of Human Evolution 42 (4): 475 -497

Berger, A.L.,1978. Long-term variations in daily insolation and Quaternary climate change. Journal of Atmospheric Science, 35: 2362-2367.

Broecker, 1994. Massive iceberg discharges as triggers for global climate change. Broecker, Nature, 372: 421-424

Broecker, W. S. 1997. Thermohaline circulation, the Achilles heel of our climate system: Will man-made CO2 upset the current balance Science 278: 1582-1588

Bond, G., Showers, W., Cheseby, M., Lotti, R., Almasi, P., deMenocal, P., Priore, P., Cullen, H., Hajdas, I., Bonani, G., 1997. A pervasive millennial-scale cycle in the North Atlantic climate during the Holocene and glacial climates. Science 278: 1257-1266.

Bond, G.C., Showers, W., Elliot, M., Evans, M., Lotti, R., Hajdas, I., Bonani, G., Johnson, S., 1999. The North Atlantic's 120 kyr climate rhythm: relation to Heinrich events, Dansgaard/Oeschger cycles and the little ice age. In: Clark, P.U., Webb, R.S., Keigwin, L.D. (Eds.), Mechanisms of Global Change at Millennial Time Scales. Geophysical Monograph 112, American Geophysical Union, Washington DC, pp. 59-76.

Bond, G., B. Kromer, J. Beer, R. Muscheler, M.N. Evans, W. Showers, S. Hoffmann, R. Lotti-Bond, I. Hajdas, and G. Bonani. 2001. Persistent Solar Influence on North Atlantic Climate During the Holocene. Science 294: 2130-2136

Bond and Lotti , 1995. Iceberg discharges into the North Atlantic on millenial time scales during the last glaciation., Science, 267: 1005-1010
Cacho, I., Grimalt, J.O., Pelejero, C., Canals, M., Sierro, F.J., Flores, J.A., and Shackleton, N.J., 1999, Dansgaard-Oeschger and Heinrich event imprints in Alboran sea paleotemperatures: Paleoceanography, 14: 698-705

Boyle, E.A., Keigwin, L.D., 1987. North Atlantic Thermohaline circulation during the last 20,000 years linked to high-latitude surface temperature. Nature 330: 35-40

Cann, R. L., Stoneking. M. and Wilson, A. C. ,1987. Mitochondrial DNA and human evolution. Nature 325: 31-36.

Chang, 1998. Unusual tropical Atlantic Ocean temperatures cause climate swings iin Brazil and West Africa. Quarterdeck 6 (2): 1 -4

Chapman and Shackleton, 1998. Millennial-scale fluctuations in North Atlantic heat flux during the last 150,000 years.Earth-and-Planetary-Science-Letters159: 57-70

Clark, P.U, Mix, A.C., 2000. Ice sheets and sea level of the Last Glacial Maximum, Quaternary Science Reviews, 21: 1-8,

Clarke, G. K. C., and La Prairie, D. I., 2001. Modelling iceberg drift and ice-rafted sedimentation. In: Continuum mechanics and applications in geophysics and the environment, edited by B. Straughan, R. Greve, H. Ehrentraut and Y. Wang, pp. 183-200, Springer-Verlag, New York.

CLIMAP, 1984. The Last Interglacial Ocean. Quaternary Research 21: 123-224

Collatz, G.J., Ball, J.T., Grivet, c., Berry, J.A., 1991. Physiological and environmental regulation of stomatal conductance, photosynthesis and transpiration: a model that includes a laminar boundary layer. Agricultural Forest Meteorology 54: 107 -136

Cox, P.M., 2001. Description of TRIFFID dynamic global vegetation model. Hadley Cell Technical Note 24: 1-16

Cox, P.M., Huntingford, C., Harding, R.J., 1999. A canopy conductance and photosynthesis model for use in a GCM land surface scheme. Journal of Hydrology 212-213: 79 -94

Dahl, K. D., Oppo, D. W., Eglinton,T. I., Hughen, K. A., Curry, W. B., Sirocko, F.,2005. Terrigenous plant wax inputs to the Arabian sea: implications for the reconstruction of winds associated with the Indian Monsoon, Geochimica et Cosmochimica Acta, 69 (10): 2547–2558

Dansgaard, W., White, J. W. C. and Johnsen, S. J. 1989. The abrupt termination of the Younger Dryas climate event. Nature, 339: 532-534.

Dansgaard, W., White, J. W. C. and Johnsen, S. J. 1993 The abrupt termination of the Younger Dryas climate event. Nature 339: 532-533.

deMenocal, P.B. ,1995.Plio-Pleistocene African climate. Science, 270: 53-59

deMenocal, P., Ortiz, J., Guilderson, T. and Sarnthein, M. 2000. Coherent high- and low-latitude climate variability during the Holocene warm period. Science 288: 2198-2202

deMenocal, P.B. 2004. African climate change and faunal evolution during the Pliocene-Pleistocene. Earth and Planetary Science. Letters, Frontiers, 6976: 1-22

Dowdeswell, J. A., M. A. Maslin, J. T. Andrews, J. T., and McCave, I. N.,1995. Iceberg production, debris rafting, and the extent and thickness of Heinrich layers (H-1, H-2) in North Atlantic sediments. Geology, 23: 301-304.

Dupont, L.M. & Hooghiemstra, H. (1989) The Saharan-Sahelian boundary during the Brunhes chron. Acta Bot. Neerl. 38/4: 405-415

Dupont, L.M. & Agwu, C.O.C.,1992. Latitudinal shifts of forest and savanna in NW Africa during the Brunhes chron: further marine palynological results from site M 16415 (9°N 19°W). Vegetation History and Archaeobotany 1: 163-175

Dupont, L.M., Jahns, S., Marret, F., Shi, N., 2000. Vegatation change in equatorial West Africa: time-slices for the last 150 ka. Paleogeography, Palaeoclimatology, Paleoecology 155: 95-122

Elenga, H., Peyron, O., Bonnefille, R., Jolly, D., Cheddadi, R., Guiot, J., Andrieu, V., Bottema, S., Buchet, G., de Beaulieu, J. L., Hamilton, A. C., Maley, J., Marchant, R., Perez-Obiol, R., Reille, M., Riollet, G., Scott, L., Straka, H., Taylor, D., Van Campo, E., Vincens, A., Laarif, F., and Jonson, H., 2000. Pollen-based biome reconstruction for southern Europe and Africa 18,000 yr BP. Journal of Biogeography 27(3): 621-634

Erlandson, Jon M. and Madonna L. Moss 2001 Shellfish Feeders, Carrion Eaters, and the Archaeology of Aquatic Adaptations. American Antiquity 66(3):413-432.

Fanning, A.F., and Weaver, A.J., 1996. An atmospheric energy-mositure balance model: climatology, interpentadal climate change amd coupling to an ocean general circulation model. Journal of Geophysical Research (atmospheres), 101 (D10): 1511-15128

Fanning, A.F., and Weaver, A.J., 1997. Thermohaline Variability: The Effects of Horizontal Resolution and Diffusion. Journal of Climate 11 (4): 709-715.

Felis, T., Lohmann, G., Kuhnert, H., Lorenz, S., Scholz, D., Patzold, J., Rousan, S.A., Al-Moghrabi, S.M., 2004. Increased seasonality in Middle East temperatures during the last interglacial period. Nature 429: 164-168

Finlayson, C., 2004. The condition in Africa and Eurasia during the Last Glacial Cycle. In: Finlayson, C., (eds) Neanderthals and Modern Humans. 135 -147. University Press, Cambridge, 2004.

Finlayson, 2005. Biogeography and evolution of the genus Homo. Trends in Ecology and Evolution, Paleontology series. 20 (8): 457 -463.

Foley, R., 1998. The Context of Human Genetic Evolution. Genome Research, 8 (4): 339-347

Frédoux, A.,1994. Pollen analysis of a deep-sea core in the Gulf of Guinea: vegetation and climatic changes during the last 225,000 years BP. Palaeogeogr., Palaeoclim., Palaeoecol. 109: 317-330

Frenzel B., 1992. Vegetation during the maximum cooling of the last glaciation. in; Frenzel B., Pecsi B & Velichko A.A.; Atlas of Palaeoclimates & Palaeoenvironments of the Northern Hemisphere. INQUA/Hungarian Academy of Sciences. Budapest.

Gabunia L, Vekua A, Lordkipanidze D, Swisher C. C, Ferring R., 2000. Earliest Pleistocene cranial remains from Dmanisi, Republic of Georgia: taxonomy, geological setting, and age. Science 288:1019-1025

Gagosian, R. B. 2003. Abrupt Climate Change: Should We Be Worried?. Woods Hole Oceanographic Institution Davos, Switzerland.

Gasse, F., 2001. Paleoclimate: Hydrological Changes in Africa. Science, 292 (5525): 2259-2260

Grimm, E.C., Jacobson, G.L. Jr.,, Watts, W.A., Hanson, B.C.S., and Maasch, K.A., 1993, A 50,000 year record of climate oscillations from Florida and its temporal correlation with the Heinrich events: Science, 261: 198-200

Grove AT, Warren A. 1968. Quaternary landforms and climate on the south side of the Sahara. Geographical Journal 134(2): 194–208.

Hastenrath, S., 1985: Climate and Circulation of the Tropics. Reidel, 455 pp.

Heinrich, H., 1988. Origin and consequences of cyclic ice rafting in the Northeast Atlantic Ocean during the past 130,000 years, Quaternary Research, 29: 142-152.

Hibler, W.D.III., 1979. A dynamic Thermodynamic sea ice model. Journal of Physical Pceanography, 9: 815 -846

Hoelzmann, P., Gasse, F., Dupont, Salzmann, L.M U., Staubwasser, M., Leuschner, D C. and Sirocko, F., 2004. Palaeoenvironmental changes in the arid and sub arid belt (Sahara-Sahel-Arabian Peninsula) from 150 kyr to present.In Battarbee, Richard W.; Gasse, Françoise; Stickley, Catherine E. (ed) Past Climate Variability through Europe and Africa. Springer, Dordrecht, The Netherlands, 219-256

Houghton, J.T., L.G. Meira Filho, J. Bruce, Hoesung Lewe, B.A. Callander, E. Haites, N. Harris, K. Maskell, (Eds), 1995. Climate Change 1994: Radiative Forcing of Climate Change and An Evaluation of the IPCC IS92 Emission Scenarios. Cambridge University Press.

Hughen, K.A., Overpeck,J.T., Peterson, L.C., and Trumbore, S., 1996. Rapid Climate Changes in the Tropical Atlantic Region during the Last Deglaciation. Nature 380: 51-54

Hughes, T.M.C., Weaver, A.J., 1994. Multiple Equilibria of an asymmetric two basin ocean model. Journal of Physical Oceanography 24: 619 -637

Hunke, E.C., and Dukowicz, J.K., 1997. An elastic-viscous-plastic model for sea ice dynamics. Journal of Physical Oceanography, 27: 1849 -1867.

Imbrie, J., J. D. Hays, D. G. Martinson, A. McIntyre, A. C. Mix, J. J. Morley, N. G. Pisias, W.L. Prell, and N. Shackleton, 1984. The Orbital Theory of Pleistocene climate: Support from a revised chronology of the marine d ^{18} O record, in Milankovitch and d ^{18} O Climate, Part 1, edited by A.L. Berger et al., pp. 269-305, D. Riedel, Hingham, Mass.

Jahns, S., Huls, M., Sarnthein, M., 1998. Vegetation and climate history of west equatorial Africa based on a marine pollen record off Liberia (site GIK 16776) covering the last 400,000 years. Review of Palaeobotany and Palynology 102: 277 -288

Jouzel, J., Barkov, N. I., Barnola, J. M., Bender, M., Chapellaz, J., Genthon, C., Kotlyakov, V. M., Lipenkov, V., Lorius, C., Petit, J. R., Raynaud, D., Raisbeck, G., Ritz, C., Sowers, T., Stievenard, M., Yiou, F., and Yiou, P., 1993, Extending the Vostok ice-coore record of palaeoclimate to the penultimate glacial period, Nature, 364: 407

Kalnay, E., M. Kanamitsu, R. Kistler, W. Collins, D. Deaven, L. Gandin, M. Iredell, S. Saha, G. White, J. Woollen, Y. Zhu, A. Leetmaa, B. Reynolds, M. Chelliah, W. Ebisuzaki, W. Higgins, J. Janowiak, K.C. Mo, C. Ropelewski, J. Wang, Roy Jenne, Dennis Joseph, 1996: The NCEP/NCAR 40-Year Reanalysis Project. Bulletin of the American Meteorological Society 77 (3): 437 -472

Kutzbach, J. E. & Liu, Z. 1997. Response of the African monsoon to orbital forcing and ocean feedbacks in the middle Holocene. Science 278: 440-444

Lahr, m.M and Foley, R., 1994. Multiple dispersals and modern human origins. Evolutionary Anthrolpolgy 3: 48 -60

Leuschner, D.C., Sirocko, F., Schettler, G., and Garbe- Schonberg, D., 2004. Geochemical implications for changing the dust supply by the Indian monsoon system for the Arabian Sea during the last glacial cycle. In : Smykatz-Kloss S., Henningsen, F., and Zoller, L. (eds). Paleoecology of Quaternary Dryland, Springer -Verlag, stuttgart.

Licciardi, J. M., J. T. Teller and P. U. Clark, 1999. Freshwater routing by the Laurentide ice sheet during the lastdeglaciation. In Mechanisms of Global Climate Change at Millennial Time Scales, AGU GeophysicalMonograph 112, P. U. Clark, R. S. Webb, and L. D. Keigwin (Eds.)

Lutze, G.F., Agwu, C.O.C., Altenbach, A., Henken-Mellies, U., Kothe, C., Mühlhan, N., Pflaumann, U., Samtleben, C., Sarntheim, M., Segl, M., Soltwedel, T., Stute, U., Tiedemann, R. & Weinholz,. P. (1988) Bericht über die METEOR-Fahrt 6-5 Dakar-Libreville 15.1-16.2.1988. Berichte Geol. Paläont. Inst. Univ. Kiel 22: 66

MacAyeal, D. R. 1993. Binge/purge oscillations of the Laurentide Ice Sheet as a cause of the North Atlantic Heinrich events, Paleoceanography, 8: 775-784.

Manabe, S., and R. J. Stouffer, 1997: Coupled ocean-atmosphere model response to freshwater input: Comparison to Younger Dryas event. Paleoceanography, 12(5): 728

Maslin, M., Trauth, M., Christensen, B., 2005. A Changing Climate For human Evolution. Geotimes: Human Evolution, Following our ancesters. 50 (9)

McDougall I, Brown F.H., Fleagle J.G., 2005. Stratigraphic placement and age of modern humans from Kibish, Ethiopia. Nature 433:733–736

McIntyre, A., Kipp, N., Crowley, T., Kellog, T., Gardner, J., Prell, W., and Ruddiman, W. (1976). Glacial North Atlantic 18,000 years ago: A CLIMAP reconstruction. In Investigations of Late Quaternary Paleoceanography And Paleoclimatology, pages 43-76. R.M. Cline und J.D. Hays, The Geological Society of America, Inc.

McManus, J.F., Bond, G., Broecker, S.J., Johnson, L., Labeyrie, S., 1994. High-resolution climate records from the North Atlantic during the last interglacial, Nature 371: 326-339

McManus, J.F., Oppo, D.W,. Cullen,J. (1999). A 0.5-Million-Year Record of Millennial-Scale Climate Variability in the North Atlantic. Science 283: 971-975

McManus, J.F., Oppo, D.W., Keigwin, L.D. and Cullen, J.L., 2000. Prolonged interglacial warmth in the North Atlantic and the onset of the last Pleistocene ice age. Quaternary Research, 58: 17-21

McManus, J.F., Oppo, D.W, Keigwin, L.D., 2002. Thermohaline Circulation and Prolonged Warmth in the North Atlantic. Quaternary Research. 58: 17-21

Meissner, K.J., Weaver, A.J., Matthews, H.D., Cox, P.M., 2003. The role of land surface dynamics in glacial inception: a study with the Uvic Earth system climate model, Climate Dynamics 21: 519-537

Nicholson, S.E., 1993. An overview of African rainfall fluctuations of the last decade. Journal of climatology, 6: 1463-1466

Oppo, D.W., J.F. McManus and J.L. Cullen. 2003. Palaeo-oceanography: Deepwater variability in the Holocene epoch. Nature, 422 (6929): 277-278 and 400

Pacanowski, R.C., 1995. MOM 2: Documentation User's Guide and Reference Manual. GFDL Ocean Group Technical Report

Partridge, T. C., DeMenocal, P. B., Lorentz, S. A., Paiker, M. J. & Vogel, J. C.,1997. Orbital forcing of climate over South Africa: a 200,000 year rainfall record from the Pretoria Saltpan. Quateranry Science Reviews 16: 1125-1133

Petit, J.R., J. Jouzel, D. Raynaud, N.I. Barkov, J.-M. Barnola, I. Basile, M. Bender, J. Chappellaz, M. Davis, G. Delayque, M. Delmotte, V.M. Kotlyakov, M. Legrand, V.Y. Lipenkov, C. Lorius, L. Pépin, C. Ritz, E. Saltzman, and M. Stievenard. 1999. Climate and atmospheric history of the past 420,000 years from the Vostok ice core, Antarctica. Nature 399: 429-436.

Porter, S.C., & An.Z.,, Correlation between climate events in the North Atlantic and China during the last glaciation, **Nature**, 375 (6529): 305-308

Prospero JM & Nees RT (1986) Impact of the North African drought and El Nino on mineral dust in the Barbados trade wind. Nature 320: 735-738

PRISM project members, 1996. Middle Pliocene paleoenvironments of the Northern Hemisphere. p. 198 -212. In; Vrba, E., Denton, g.h., Partridge, T.C. & Burckle, L.H. Plaeoclimate and Evolution, with emphasis on human origins. Yale University Press, New Haven.

Quintana-Murci, L., Semino, O., Bandelt, H.,, Passarino, G., McElreavey, K., Santachiara-Benerecetti, S., 1999. Genetic evidence of an early exit of Homo sapiens sapiens from Africa through eastern Africa. Nature Genetics 23: 437 - 441

Rahmstorf, S., 2003: Thermohaline circulation: The current climate. Nature 421, 699

Raymo, M.E., 1994. The initiation of Northern Hemisphere glaciation, Annu. Rev. Earth Planet. Science. 22: 353-383.

Rasmusssen, T. L, Oppo D. W., Thompson E., Lehman, J., 2003. Deep sea records from the southeast Labrador Sea: Ocean circulation changes and ice-rafting events during the last 160,000 years, Paleoceanography 18 (1)

Reichart, G.J., Lourens, L.J., and Zachariasse, W.J., 1998. Temporal variability in the northen Arabian Sea Oxygen minimum zone during the last 225,000 years. Paleooceanography 13: 607 – 621

Ruddiman, W.F, Raymo, M.E., Martinson, D.G. Clement, B.M., Backman, J., 1989. Pleistocene evolution: Northern Hemisphere ice sheets and North Atlantic Ocean, Paleoceanography 4: 353-412.

Sauer, C. O., 1962. Seashore - primitive home of man? Proceedings of the American Philosophical Society 106: 41–7.

Schiller, A., Mikolajewicz, U. and Voss, R. 1997. The stability of the thermohaline circulation in a coupled ocean-atmosphere general circulation model. Climate Dynamics 13: 325-348.

Scheub, E., Schouten, S., Schneider, R., 2005. Climate Controls on Central African Hydrology during the past 20,000 years. Nature 437 (13): 1003 -1006

Schulz, H., Rad, U., Erlenkeuser, H., 1998. Correlation between Arabian Sea and Greenland climate oscillations of the past 110,000 years. Nature 393: 54 - 57

Semtner. A.J.Jr., 1976. A model for the thermodynamic growth of sea ice in numerical investigations of climate. Journal of Physical Oceanography, 6: 379 -389

Shackleton NJ, Hall MA, 1984, Oxygen and carbon isotope stratigraphy of Deep Sea Drilling Project Hole 552A: Plio-Pleistocene glacial history. Initial Rep. of the Deep Sea Drilling Project 81:599-610

Shackleton, N.J., A. Berger, A.,Peltier, W.R., 1990. An alternative astronomical calibration of the lower Pleistocene timescale based on ODP Site 677, Trans. R. Soc. Edinburgh Earth Science 81: 251-261.

Shackleton, N. and Opdyke, N. ,1973. Oxygen isotope and paleomagnetic stratigraphy of Equatorial Pacific core V 28-238: Oxygen isotope temperature and ice volumes on a 10^6 year scale. Quaternary Research, 3:39-55.

Singer, R. and Wymer, J. 1982. The Middle Stone Age at Klasies River Mouth in South Africa. University of Chicago Press.

Stringer, C., and Andrews, P. 1988. Genetic and fossil evidence for the origin of modern humans. Science 239:1263-1268.

Stringer, C. B., 1990. The emergence of modern humans. Science America : 98–104.

Stringer C., 2000. Coasting out of Africa. Nature 405: 24–27.

Stringer, C.B., 2000. The Evolution of Modern Humans. Where are we now? General Anthropology 7 (2): 1-5.

Stokes, S., Thomas, D.S.G., Washington, R.,1997. Multiple episodes of aridity in southern Africa since the last interglacial period. Nature 388:154-8.

Swezey, C., 2001, Eolian sediment responses to late Quaternary climate changes: Temporal and spatial patterns in the Sahara: Palaeogeography, Palaeoclimatology, Palaeoecology 167: 119-155.

Thorne, A. and Wolpoff, M.H. 1992. The multiregional evolution of humans. Scientific American 266: 76-83.

Tiedemann, R., M. Sarnthein, and N. J. Shackleton, 1994. Astronomic timescale for the Pliocene Atlantic d18O and dust flux records of ODP Site 659, Paleoceanography, 9(4), 619-638

Trinkaus, Erik, 1986. The Neanderthals and Modern Human Origins, Annual Review of Anthropology, 15:193-218.

Van Andel T.H. & Tzedakis P.C.,1996. Palaeolithic landscapes of Europe and environs: 150,000-25,000 years ago: an overview. Quaternary Science Reviews. 15: 481-500.

Van Campo, E., Duplessy, J.C. & Rossignol-Strick, M. (1982) Climatic conditions deduced from 150-Kyr oxygen isotope-pollen record from the Arabian Sea. Nature 296: 56-59

Vidal L. and Arz, H., 2004. Oceanic climate varaibility at Millenial ttime scale : modes of climate connections, in Battarbee, R.W., F. Gasse and C. Stickley (Eds), Past climate variability through Europe and Africa, Springer, Dordrecht, the Netherland

Vrba, E.S., Denton,G.H., and Prentice, M.L., 1989. Climatic influences on early Hominid behavior, Ossa, 14: 127-156.

Vrba, E.S.,1995. The fossil record of African antelopes (Mammalia, Bovidae) in relation to human evolution and paleoclimate. pp 385-424 in Vrba, E.S., Denton G.H., Partridge, T.C., (eds: Paleoclimate and Evolution. Yale University Press, New Haven and London, 1996.

Walter, R.C., Buffler, R.T., Bruggemann, J.H., Guillaume, M.M.M., Berhe, S.M., Negassi, B., Libsekal, Y., Cheng, H., Edwards, R. L., Cosel, R., Néraudeau, D., Gagnon,M., 2000. Early human occupation of the Red Sea coast of Eritrea during the last interglacial Nature 405: 65-69

Weaver, A.J., Eby, M., Wiebe, E.C., Bitz, C., Duffy, T.E., Fanning, M.H., MacFadyen,A., Matthews, H.D., Meissner, K.J., Saenko, O., Schmittner, A., Wang, H.., Yoshimori, M., 2001. The UVic Earth System Climate Model: Model Description, Climatology and Applications to Past, Present and Future Climates. Atmosphere-Ocean, 39(4): 361-428.

White TD, Asfaw B., DeGusta D., Gilbert H., Richards GD, Suwa G., 2003. Pleistocene Homo sapiens from Middle Awash, Ethiopia. Nature, 423:742-7.

Wilson, M. F., and A. Henderson-Sellers, 1985: A global archive of land cover and soils data for use in general circulation climate models. J. Climatol., 5, 119-143.

Woodward F. I., Lomas M. R., Kelly C. K., 2004. Global climate and the distribution of plant biomes, Philosophical Transactions of the The Royal Society. 359:1465-1476

Zhao, M., Dupont, L., Eglinton, G., Teece, M., 2003. N-alkane and pollen reconstruction of terrestrial climate and vegetation for Northwest Africa over the last 160 kyr. Organic Geochemistry 34, 131 -143